Carbon 214 (2023) 118358

Contents lists available at ScienceDirect

Carbon

journal homepage: www.elsevier.com/locate/carbon

Stability of destructive quantum interference antiresonances in electron transport through graphene nanostructures

Angelo Valli [a,b,*], Thomas Fabian [a], Florian Libisch [a], Robert Stadler [a]

[a] Institute for Theoretical Physics, Vienna University of Technology, Wiedner Hauptstrasse 8-10, Vienna, 1040, Austria
[b] Department of Theoretical Physics, Institute of Physics, Budapest University of Technology and Economics, Müegyetem rkp. 3, Budapest, 1111, Hungary

ARTICLE INFO

Keywords:
Graphene
Quantum transport
Quantum interference

ABSTRACT

We investigate the stability of destructive quantum interference (DQI) in electron transport through graphene nanostructures connected to source and drain electrodes. The fingerprint of DQI is an antiresonance in the transmission function, and its origin is deeply connected to the topology of the atomic structure, which we discuss in terms of symmetry arguments supported by numerical simulations. A systematic analysis of the transmission function versus system size reveals that the DQI antiresonance persists for large systems in the ballistic regime and establishes the quantum confinement gap as the intrinsic resolution limit to detect QI effects. Furthermore, we consider the influence of disorder, electron–electron and electron–phonon interactions, and provide quantitative criteria for the robustness of DQI in their presence. We find that the conductance is quite sensitive to perturbations, and its value alone may not be sufficient to characterize the quantum interference properties of a junction. Instead, the characteristic behavior of the transmission function is more resilient, and we suggest it retains information on the presence of an antiresonance even if DQI is partially concealed or suppressed. At the same time, DQI results in a non-linear transport regime in the current-bias characteristics that can be possibly detected in transport experiments.

1. Introduction

Quantum interference (QI) in electron transport is a purely quantum mechanical phenomenon of keen interest in the field of molecular electronics. In single-molecule junctions, experimental evidence of both destructive [1–6] (DQI) and constructive [7–9] (CQI) quantum interference, as well as their control [10,11] has been extensively reported. Sharp antiresonances due to QI with asymmetric Fano shapes and symmetric Mach–Zehnder shapes can be found and theoretically explained [12–18]. Close to the Fermi level, sharp antiresonances drastically affect the transport properties [19–22], and indeed, QI has been proposed as a paradigm for a wide spectrum of technological applications, ranging from logic gates [15,23] single-molecule transistors [24,25], molecular switches [5,26], spin-filters [27–30], as well as for enhancing the performance of thermoelectric [4,8,31,32] and chemical sensing [21,33,34] devices.

Fundamentally, QI effects occur when the transmission of electrons across a resistor is phase-coherent, which is realized when the length of the transmission channel $\mathcal{L}$ is shorter than the characteristic scale (mean free path) associated with elastic (λ_e) and phase-breaking (λ_ϕ) electron scattering events, i.e., $\mathcal{L} < \lambda_e, \lambda_\phi$ (ballistic regime). For large ballistic cavities of size $\mathcal{L}$, an intuitive interpretation is provided by semiclassical approaches like Gutzwiller's trace formula [35]. By contrast, QI in the context of molecular electronics rather originates from contributions between different molecular orbitals (MO), depending on their coupling strength to the electrodes and their phases [36,37]. A qualitative understanding of QI can be achieved within a single-particle picture, thus making QI deceptively simple. However, careful treatment is warranted, since the loss of electronic phase coherence is typically (but not exclusively) associated to inelastic processes which are often neglected in theoretical calculations, such as, e.g., electron–electron or electron–phonon scattering.

Notwithstanding different sources of scattering, which can possibly spoil phase coherence, QI effects can be detected under experimental conditions. While early evidence of QI has been rather indirect [38], the dramatic technological progress of the last few decades eventually lead to a clear direct detection of DQI [1,5,6].

It is worth stressing that, while the synthesis of molecular bridges is very advanced, current junction fabrication techniques do not offer high enough spatial resolution to reliably contact single molecules within well-defined geometries. Instead, transport measurements of

* Corresponding author at: Department of Theoretical Physics, Institute of Physics, Budapest University of Technology and Economics, Müegyetem rkp. 3, Budapest, 1111, Hungary.
E-mail address: valli.angelo@ttk.bme.hu (A. Valli).

https://doi.org/10.1016/j.carbon.2023.118358
Received 21 March 2023; Received in revised form 11 July 2023; Accepted 6 August 2023
Available online 10 August 2023

single-molecule devices are typically performed with break-junction techniques, either in a mechanically-controlled or a scanning tunneling microscope setup [39]. In the simplest case, a thin gold wire is mechanically strained until the wire breaks, creating two fresh electrode surfaces that can now be connected by individual molecules in a self-assembled way. Consequently, the junction is subject to configuration fluctuations, as the atomic arrangement is unknown. The measurement is therefore repeated over a series of break-junction events to obtain reliable statistics. Despite the statistical nature of break-junction experiments, there are protocols to identify the suppression of electron transmission due to DQI, e.g., in differential conductance (dI/dV_b) maps [1,40,41], or through the analysis of conductance histograms [2,6,11,42,43] of single-molecule junctions. Remarkably, QI effects seem also to be surprisingly stable, having been detected even at room temperature [1,9,10,43], and on length scales well beyond that of single-molecule junctions, in systems such as, e.g., macromolecules [44] as well as nanostructured graphene [19,28,29,45,46].

In particular, graphene represents a natural platform for high-performance nanoelectronics [47], thanks to its unique physical properties, and its ability to form atomically precise nanostructures [46,48–51]. Antiresonances akin to those occurring in single-molecule junctions have been predicted theoretically [28,29,52–58] and confirmed experimentally [19,46,59–61]. QI effects can also occur in the diffusive regime, i.e., $\lambda_e \ll \mathcal{L} < \lambda_\phi$, where weak localization can arise due to the coherent superposition of random scattering paths [62]. Since the effective mean free path of electrons in graphene strongly depends on the local doping [63], both regimes may be relevant for a single device at different energies.

In the present work we analyze, within a unified framework, the stability of QI antiresonances in graphene nanostructures. We show that the ballistic transmission function displays a characteristic behavior within the quantum confinement gap, that can be entirely ascribed to the existence of an antiresonance. We consider a wide range of different mechanisms which are detrimental to QI, including disorder, electron–electron, and electron–phonon interactions, and quantify their effect on a QI antiresonance. Our results thus provide stringent boundaries on the possibility of detecting QI effects in an experimentally-relevant parameter range.

2. Topological conditions for DQI

Predicting the occurrence of QI in the electron transmission function is a challenging task [12,23,64–67]. A few *back-of-the-envelope* methods have been developed [14,23,64,66,68,69], including a graphical scheme, which relies on a visual inspection of the molecular structure and the topology of the Hückel (or tight-binding) Hamiltonian, and is able to predict DQI without the need for explicit numerical simulations [23]. This graphical scheme has been validated against density functional theory [64], it was extended to hetero-atoms [65], non-alternant hydrocarbons such as azulene [66,67], and further generalized in a diagrammatic fashion to calculate the position of the antiresonances [66]. The Coulson–Rushbrooke pairing theorem from quantum chemistry [70] has recently reconciled the graphical approach with a MOs perspective more common for a theoretical analysis of molecular properties [36].

The graphical scheme and the pairing theorem naturally link the sublattice structure to DQI. The term alternant hydrocarbons refers to conjugated hydrocarbon systems where carbon atoms can be divided into two subsets (or sublattices) with nearest-neighbor interactions only between two atoms of the two different subsets – i.e., any hydrocarbon system containing no odd-membered rings. For such systems a QI antiresonance appears between the highest occupied (HOMO) and the lowest unoccupied (LUMO) MOs if the contact sites belong to the same sublattice [28,29,36,58,71,72]. If the contact sites belong to different sublattices, DQI is still possible if certain conditions are met [58], but it is in general harder to predict. These properties have also been confirmed within the more general framework of Green's functions formalism, [28,29,57,58,73,74] which also revealed a rich QI phenomenology [74]. Specifically, DQI has been demonstrated numerically for rectangular [57,58] and hexagonal [28,29] graphene nanostructures. Indeed, such an argument predicts DQI in graphene nanostructure with any size and shape, with some *caveats* [58,73]. Since graphene nanostructures can be considered, and even chemically synthesized [48,75], as extended polyaromatic molecules with an alternant structure and hydrogen-passivated edges, the sublattice scenario naturally holds. While selectively contacting a specific sublattice can be difficult from the experimental point of view, it is within reach of present fabrication technologies. For instance, linker molecules are routinely used in single-molecule mechanically-controlled break junctions. They act as *spacer* allowing the molecule to bridge the nano-gap between the electrodes and at the same time can be used to target specific C atoms for contacting the electrodes. In this sense, the choice of considering nanostructures with zig-zag edges is very natural, as all C atoms along a given zig-zag edge (i.e., those available to bond to either passivating groups or to the linkers) belong to the same sublattice. This is expected to facilitate contacting in an experimental setup. Provided that the contacting can be engineered to be atomically precise, DQI can arise independently on the edge topology of edges (e.g., zig-zag, armchair, or even imperfect ones). Another interesting case is that of imperfections, such as Stone–Wales (pentagonal-heptagonal) defects and vacancies, due to which the sublattice symmetry is locally broken. A graph theoretical analysis of QI has been proposed [73] to treat these scenarios in terms of perturbations of a bipartite subsystem (for which the QI properties are known or easy to predict). Some perturbations leave the interference set invariant, while others lift or create additional antiresonances. However, with state-of-the-art bottom-up fabrication technologies, especially those based on molecular precursors, it is possible to realize defect-free, atomically-precise graphene nanostructures, with a variety of edge termination [48]. From this perspective, an analysis of QI effects in graphene nanostructures without intrinsic lattice imperfections is still experimentally relevant.

The topological argument greatly simplifies the theoretical analysis and, at the same time, can guide the experimental fabrication, as it provides a very simple criterion to identify which contact configurations display a QI antiresonance. It is equally clear, however, that for larger graphene flakes with several transmission channels, more phases accumulate, and as a consequence, the characteristic dip due to DQI becomes less pronounced. Indeed, only the existence of the dip is topologically protected — there is no general statement on its width. Additional interactions such as electron–electron or electron–phonon coupling will further affect the phase coherence required for quantum interference effects. Consequently, one might ask under which realistic conditions DQI effects can still be measured. In the following, we intend to provide a comprehensive answer to this question, investigating the role of system size, disorder, electron–phonon, and electron–electron coupling on the DQI dip.

3. Results

We consider a graphene nanostructures with rhomboidal shape and size $N\times N$, where N denotes the number of rings along each edge, and n_C the number of C atoms in the nanostructure (see Fig. 1a). As we discuss below, our arguments are rather general and are expected to remain valid for graphene nanostructure with other shapes (e.g., rectangular or hexagonal). Let us further denote by $\{\ell\} = \{\ell_1, \ell_2, \ldots\}$ and $\{r\} = \{r_1, r_2, \ldots\}$ the sets of edge AOs contacted to the L and R leads, respectively. We indicate as *meta* and *para* the configurations in which the atoms in sets $\{\ell\}$ and $\{r\}$ belong to the same or opposite graphene sublattices (see Fig. 1c). Here we just focus on the graphene nanostructure and the contact atoms therein, independently on the particular experimental strategy that can be employed to create the junction and contact the bridge to the electrodes, e.g., introducing

linkers and anchoring groups, and we implicitly assume that those elements do not introduce QI features.

We begin our analysis by studying the dependence of DQI features on system size within the tight-binding approximation. The corresponding Hamiltonian, describing a single p_z AO per C atom, reads

$$\mathcal{H}_0 = t \sum_{\langle ij \rangle} \sum_{\sigma} c^{\dagger}_{i\sigma} c_{j\sigma}, \tag{1}$$

where $c^{(\dagger)}_{i\sigma}$ is the annihilation (creation) operator for an electron at site i with spin σ, and t is the hopping between nearest-neighbor sites i and j, for which we take a typical value $t = 2.7\,\mathrm{eV}$. Including longer-range hoppings, or deriving them *ab-initio* [76], e.g., breaks the particle-hole symmetry and shifts the position of the antiresonance within the gap [28] but does not invalidate our conclusions (see also our analysis in the presence of disorder).

Since the tight-binding Hamiltonian $\mathcal{H}_0$ does not include any scattering mechanism (neither elastic nor inelastic), in this approximation the electronic excitations do not decay, i.e., are characterized by a lifetime $\tau = \infty$ and mean-free paths $\lambda_e = \lambda_\phi = \infty$. As we introduce disorder, electron–electron, or electron–phonon scattering below, we estimate the characteristic length scales on which QI effects are suppressed.

3.1. Universal transport behavior due to DQI

We describe electronic transport within the Landauer formalism [77], where the transmission function is given by

$$T(\omega) = \mathrm{Tr}\left[\Gamma^L(\omega) G^{\dagger}(\omega) \Gamma^R(\omega) G(\omega)\right], \tag{2}$$

in terms of the molecular Green's function $G(\omega)$ and the coupling matrix $\Gamma^{L/R}$ to the left (L) and right (R) leads. We assume that the leads-molecule coupling is diagonal in the AO indices, i.e., $\Gamma^L_{\ell\ell'} = \Gamma\delta_{\ell\ell'}$ and $\Gamma^R_{rr'} = \Gamma\delta_{rr'}$, and we further employ a wideband limit (WBL) approximation for the leads, so that the coupling elements $\Gamma^L_{\ell\ell}$ and Γ^R_{rr} are given by energy-independent constants Γ for edge C atoms in the sets $\{\ell\}$ and $\{r\}$, and zero otherwise, see also Supplementary Material (SM). In the following, we set all non-zero couplings to the leads to $\Gamma = 0.0004t \approx 1\,\mathrm{meV}$ (or $\approx 10\,\mathrm{K}$, for reference) and we focus on the non-resonant transport regime. We have verified numerically that neither the WBL approximation [28,78,79] nor neglecting non-diagonal couplings $\Gamma_{i\neq j}$ [17,80–82] fundamentally change the QI properties of the system under study. Under the assumptions above, we can decompose the transmission function as a sum over *independent* transmission channels

$$T(\omega) = \sum_{\ell r} T_{\ell\to r}(\omega) = \Gamma^2 \sum_{\ell r} |G_{\ell r}(\omega)|^2. \tag{3}$$

In the non-resonant transport regime, the condition for an antiresonance in a given channel $T_{\ell\to r}$ due to DQI becomes $\Re G_{\ell r}(\omega_{\mathrm{DQI}}) = 0$, for a given frequency ω_{DQI} [28,29,74]. While ω_{DQI} can be different in each channel, due to the particle-hole symmetry of Hamiltonian (1) the antiresonance is *pinned* at $\omega_{\mathrm{DQI}} = 0$ in each channel. In Figs. 1(b,d) we show the *total* transmission function, i.e., the sum over all possible contributions $T_{\ell\to r}$ for the 4×4 graphene nanostructure. Indeed, we find a pronounced antiresonance at $\omega = 0$ (solid line in Fig. 1b) if $\{\ell\}$ and $\{r\}$ belong to the same sublattice (labeled as *meta* configuration, Fig. 1c). If $\{\ell\}$ and $\{r\}$ instead belong to different sublattices (labeled as *para* configuration, Fig. 1c) we find no antiresonance, and the transmission function within the HOMO-LUMO gap saturates at a much higher value (dashed line in Fig. 1b). These results are consistent with the topological conditions for DQI discussed above.

In the meta configuration, we identify a *universal* behavior of the transmission function and we show that it can be ascribed to the presence of the DQI antiresonance. We calculate the transmission function through graphene nanostructures of increasing size and we show $T(\omega > 0)$ on a log–log scale (Fig. 1d). Due to the particle-hole symmetry in our model, the transmission function is symmetric, i.e., $T(-\omega) = T(\omega)$ and the antiresonance is *pinned* at $\omega_{\mathrm{DQI}} = 0$ [29]. The transmission function saturates close to the antiresonance $\omega \to \omega_{\mathrm{DQI}}$ whereas it is unitary in correspondence to the LUMO resonance at ω_{LUMO}. The evolution of ω_{LUMO} shows that the HOMO-LUMO gap $\Delta_0 = \omega_{\mathrm{LUMO}} - \omega_{\mathrm{HOMO}}$, decreases with systems size (see also Fig. 1e), in agreement with the literature [83–85]. At intermediate energies, we find that the transmission follows the universal behavior

$$T_{\mathrm{meta}}(\omega) \sim \Gamma^2 \left[\alpha_0^2 + \alpha_1^2 \omega^2\right], \tag{4}$$

where α_k is the (size-dependent) real-valued coefficient of the ω^k term in the expansion of the Green's function. Such behavior follows naturally upon symmetry considerations. Indeed, when ℓ and r belong to the same sublattice, it can be shown [29] that: (i) $\Re G_{\ell r}(\omega)$ and $\Im G_{\ell r}(\omega)$ are odd and even functions of ω, respectively, and (ii) $\Re G_{\ell r}(0) = 0$, which defines ω_{DQI}. Hence, to the leading order $G_{\ell r}(\omega) \sim \alpha_1\omega + \imath\alpha_0$. Inserting the expansion of the Green's function in Eq. (3) yields Eq. (4) and the universal behavior of the transmission function (see the SM for a detailed derivation). Remarkably, we verify numerically that the leading order dominates not only close to ω_{DQI} but it extends on a wider window within the HOMO-LUMO gap. Deviations from this behavior are observed when contributions from the frontier MO resonances become sizable. While it is convenient to derive the universal behavior from symmetry considerations, we verify numerically that it holds even when the particle-hole symmetry is broken and it can therefore be expected also for realistic nanostructures beyond our minimal tight-binding model (see, e.g., Fig. 2d and the analysis in the presence of disorder).

From the numerical data we observe a weakly size-dependent saturation value $T(\omega_{\mathrm{DQI}})$. However, at a finite energy scale, e.g., due to experimental resolution, the transmission increases approximately by an order or magnitude when increasing N by one unit. This is because Δ_0 decreases with size but the coupling between molecule and leads Γ, which determines the width of the transmission features, remains constant. An analogous dependence of the transmission function is observed at constant Δ_0 by increasing Γ (see SM). To remove this contribution, we consider the ratio $\xi(\omega) = T_{\mathrm{meta}}(\omega)/T_{\mathrm{para}}(\omega)$ between the transmission in the meta and para configurations (Fig. 1f). Away from the Dirac point, i.e., for $|\omega/t| \gg 0$ the transmission in meta and para configurations approach each other, $\xi(1) \to 1$ because the position and the width of the LUMO and HOMO resonances are the same in the meta and para configurations (Fig. 1b). For energies within the HOMO-LUMO gap, all the curves $\xi(\omega)$ *collapse* onto each other (see Fig. 1f). We ascribe the imperfect collapse at $N \leq 4$ to the distribution of poles of the transmission function on the complex plane. Hence, by disentangling the behavior induced by the antiresonance from Δ_0 and Γ, we can draw the following conclusions: (i) for $N \geq 4$, the transmission T_{meta} within the HOMO-LUMO gap approaches the universal form of Eq. (4), with the prefactor α_1 determined by $T_{\mathrm{meta}}(\omega_{\mathrm{LUMO}}) = T_{\mathrm{para}}(\omega_{\mathrm{LUMO}})$ (i.e., $\xi(\omega_{\mathrm{LUMO}}) \to 1$), and (ii) our argument remains valid for differently shaped graphene nanostructures, especially as the surface-to-bulk ratio decreases. Hence, in the following, we shall focus on a 4×4 graphene nanostructure, which strikes a good balance between numerical cost while displaying weak-to-none finite-size effects on the universal behavior of the transmission of Eq. (4).

Remarkably, the universal behavior of the transmission function reflects on the current-bias ($I - V_b$) characteristics, which can be directly measured in the experiment, whereas the transmission is loosely related to the differential conductance dI/dV_b, at least at low bias voltages $eV_b = \mu_L - \mu_R$, where μ_L (μ_R) is the chemical potential in the left (right) contact. We model the bias dependence in the Landauer–Büttiker framework, i.e.,

$$I \approx \frac{e}{h} \int_{\mu_R}^{\mu_L} T(\omega)\mathrm{d}\omega, \tag{5}$$

where e denotes the electric charge and h the Planck constant. Within the HOMO-LUMO gap, we can insert the universal behavior of the

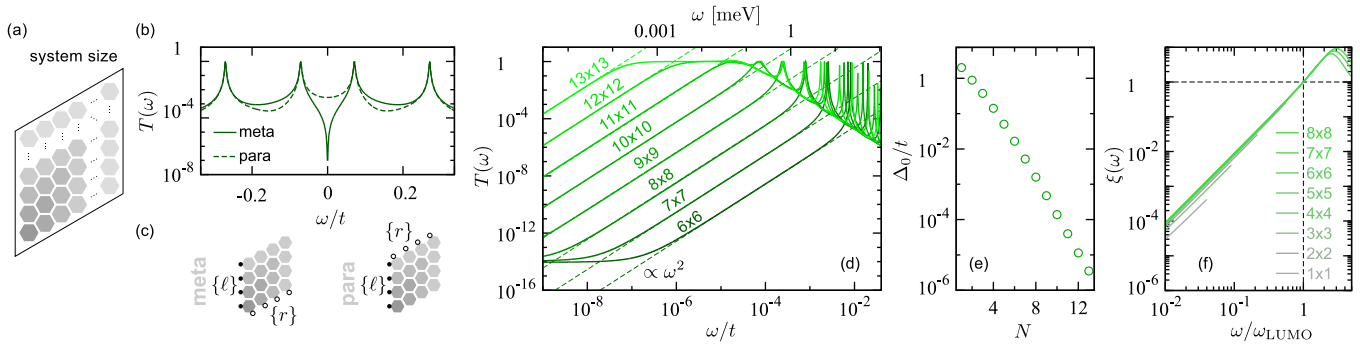

Fig. 1. Effects of system size on DQI. (a) Representative $N \times N$ graphene nanostructure. (b) Transmission function in the meta an para configurations for a 4×4 nanostructure. (c) Connections in the meta and para configurations, the black and white circles indicate the sets of AO $\{\ell\}$ and $\{r\}$ connected to the L and R leads, respectively. (d) Evolution of the transmission function in the meta configuration with system size. Within the gap $T(\omega) \propto \omega^2$ and saturates as $\omega \to \omega^{\rm DQI}$. (e) Evolution of the HOMO-LUMO gap Δ_0 with system size. (f) Data collapse of the ratio ξ between the transmission function in the meta and para configurations, for system size $N \gtrsim 4$. (For interpretation of the references to color in this figure legend, the reader is referred to the web version of this article.)

transmission function. For the meta configuration, $I_{\rm meta} \propto V_b$ only close to the antiresonance, whereas when the ω^2 behavior of Eq. (4) supersedes, it yields a non-linear characteristic $I_{\rm meta} \propto V_b^3$. In the para configuration the slowly-varying transmission $T_{\rm para}(\omega) \approx$ const results in a linear characteristic $I_{\rm para} \propto V_b$ (see SM). Hence, we identify this specific non-linear transport regime as a fingerprint of DQI, which is useful for the experimental characterization of a junction, besides the value of the zero-bias conductance $G = (e^2/h)T(0)$. Indeed, recent experimental investigations [5,40,86] have suggested non-linear $I-V_b$ characteristics to originate from DQI features in the electron transmission, whereas it is not found for molecular bridges missing a DQI antiresonance or when the antiresonance lies far from the Fermi energy of the electrodes [40]. In the latter case, while displaying a linear $I-V_b$ characteristic, the influence of QI effect can be still detected in the thermoelectric properties, as, e.g., the Seeback coefficient is sensitive to the asymmetric slope generated by a DQI antiresonance away from the Fermi energy [86].

In single-molecule junctions, with a gap in the range of a few eV, the experimental resolution necessary to resolve the in-gap $I-V_b$ characteristics is hardly an issue. By contrast, the HOMO-LUMO gap quickly becomes unmeasurably small for large graphene nanostructures, i.e., below 1 meV for $N = 11$. Another possible limitation is the contribution to the transmission function through the σ channel, which is neglected in our numerical simulation, and can in principle mask interference effects in the π channel. However, the σ contribution is naturally suppressed for longer molecules due to a faster decay with length (see, e.g., [87] and references therein) and can therefore be expected to be less relevant upon increasing systems size.

In summary, for larger flakes, the main restriction for observing DQI effects is the energy scale of the HOMO-LUMO gap, which approaches the limit of experimental resolution at $N \gtrsim 12$.

3.2. Disorder

For exploiting DQI in practice, robustness with respect to moderate disorder is critical. Sources of disorders can be intrinsic or extrinsic. Intrinsic disorder is related to defects in the crystal structure, e.g., vacancies, edge or Stone–Wales (pentagonal-heptagonal) defects, whereas extrinsic disorder originates from the environment, including strain and impurities from the substrate and adsorbates (e.g., due to oxidation). With state-of-the-art bottom-up fabrication technologies, especially those based on molecular precursors, it is possible to realize defect-free, atomically-precise graphene nanostructures, with a variety of edge terminations [48]. In mechanically exfoliated graphene most of the disorder is extrinsic [51,88]. In contrast to earlier devices on SIO_2 substrates, exhibiting chemical potential variations of ~ 100 meV, in state-of-the-art graphene devices sandwiched between hexagonal boron-nitride (hBN) bulk disorder is of the order of a few meV [51], with a major contribution from long-range strain modulations [89], and evidence of ballistic transport exceeding 1 μm has been reported [90]. For graphene nanostructure with length scales of a few nm there are no experimental reference values. The dominant source disorder is likely the different chemical environment at edge C atoms due to passivation (with H or other functional groups). Some insight comes from density functional theory, suggesting that passivation with different atoms induces a charge redistribution in the proximity of the edges, and a corresponding change in the energy of the frontier MOs of the order of 100 meV [85]. Notwithstanding, transport simulations for graphene-like molecules such a pyrene [34,79] or anthanthrene [14], find the DQI antiresonance not far from the middle of the HOMO-LUMO gap.

We investigate the influence of uncorrelated local random disorder focusing on the configurations exhibiting DQI. The scope of our analysis is two-fold: (i) we show how the transmission function changes with respect to the pristine sample, for configurations with *static* disorder, and (ii) we look at the transmission function averaged over hundreds of disorder realizations (also referred to as *dynamic* disorder) by adding the individual transmission traces incoherently. The disorder average is representative of the statistical nature of experimental measurements in a break-junction setup. The combination of the two effects allows us to understand the stability of DQI against disorder. We find that QI is surprisingly robust up to disorder amplitudes of ≈ 40 meV, which is at least one order of magnitude above the experimental estimates for state-of-the-art devices.

The local disorder is described by adding to the tight-binding Hamiltonian (1) the following term

$$\mathcal{H}_{\rm disorder} = \sum_{i\sigma} \epsilon_i n_{i\sigma}, \tag{6}$$

where $n_{i\sigma} = c_{i\sigma}^\dagger c_{i\sigma}$ is the number operator and ϵ_i is the on-site energy of site i. We create random disorder with $\langle \epsilon_i \rangle = 0$ and $\langle \epsilon_i^2 \rangle = A^2$, with A the disorder amplitude. Such a local potential is suitable to describe extrinsic disorder such as chemical potential fluctuations. Moreover, the disordered nanostructure is generally not at half-filling, it also describes doping effects due to charge transfer between the graphene structure and adsorbate atoms and molecules.

We calculate the transmission function for different disorder realizations (Fig. 2). Since disorder breaks the particle-hole symmetry, the energies of the MOs, and their projection onto the C-p_z AOs no longer fulfill the Coulson–Rushbrooke pairing theorem. In particular, the position of the frontier MOs ($\omega_{\rm HOMO}$ and $\omega_{\rm LUMO}$) now depends on the specific disorder realization, shifting the characteristic DQI dip in the transmission function randomly (Fig. 2b). The antiresonance, which emerges from the cancellation of contributions involving all MOs [36], is no longer pinned at the Fermi energy, i.e., $\omega_{\rm DQI} \neq 0$. Moreover, the cancellation of the transmission is partial. In order to better understand

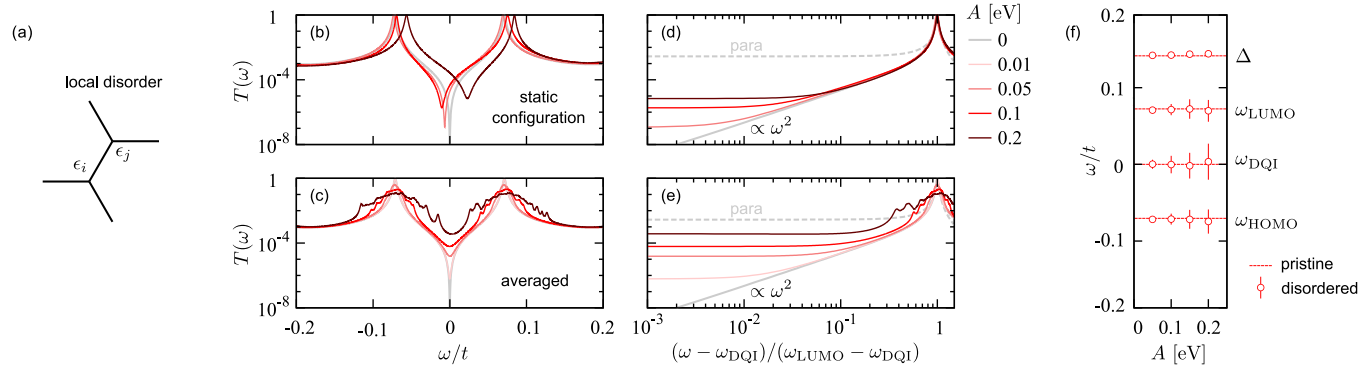

Fig. 2. (a) Schematic representation of the local disorder. (b,c) Transmission function for a specific disorder realization (b) and averaged over hundreds of realizations (c), for different values of disorder strength. (d,e) Rescaling the energy allows aligning the position of the antiresonance $\omega_{\rm DQI}$ and of the LUMO resonance $\omega_{\rm LUMO}$ for each disorder realization (or their average). Disorder strongly enhances the conductance, but the characteristic ω^2 behavior is clearly observed over an extended energy range up to moderate disorder strength. Dashed gray lines mark the transmission functions of the corresponding pristine para configurations as a reference. (f) In contrast to the other transmission features whose variance increases with the disorder strength, a statistical analysis reveals that the size of the HOMO-LUMO gap is remarkably stable around the pristine values (red dashed lines). (For interpretation of the references to color in this figure legend, the reader is referred to the web version of this article.)

this result, we recall that, in the pristine case, each transmission channel $T_{\ell\to r}$ exhibits a *sharp* DQI antiresonance at $\omega_{\rm DQI}=0$ due to the particle-hole symmetry (this is also demonstrated numerically in the SM). In the presence of disorder, the particle-hole symmetry is broken and each contribution $T_{\ell\to r}$ in the meta configuration exhibits a *sharp* DQI antiresonance at a different energy (i.e., $\omega_{\rm DQI}$ becomes channel dependent) determined by the specific realization of the disorder potential (see SM). Hence, the total transmission function displays a *broader* DQI suppression, given by the contribution of several antiresonances at different energies. The broadening depends on the distribution of the individual antiresonances and therefore on the strength of the disorder potential.

We also mention that the shift of the DQI antiresonance position due to the interaction of the surface and an adsorbate, and the corresponding chemiresistive response, is the underlying mechanism of QI chemical sensors [33,34].

Averaging over disorder further smears out the signatures of DQI (Fig. 2c). Close to the DQI resonance, the conductance is thus effectively *enhanced* by disorder, both in individual realizations (as the antiresonance shifts away from the Fermi energy) and on average. In this sense, we can talk about *disorder-assisted* transport, as the role of the disorder is to suppress the QI effects responsible for the transmission minimum. Finally, we note that for individual realizations the resonant transport through the MOs remains unitary, while the average over disorder introduces an effective decoherence and drives the system away from the ballistic regime.

In order to understand how disorder affects the universal behavior of the transmission function, we rescale the conductance traces as a function of the dimensionless scale $(\omega-\omega_{\rm DQI})/(\omega_{\rm LUMO}-\omega_{\rm DQI})$, using the corresponding value of $\omega_{\rm DQI}$ and $\omega_{\rm LUMO}$ extracted for each individual disorder realization (Fig. 2d) or their average (Fig. 2e). This aligns the position of both the antiresonance and the gap edge for both static and dynamic disorder. Focusing on the transmission function close to the antiresonance, we find quadratic enhancement with disorder strength, i.e., $T(\omega_{\rm DQI})\propto A^2$ for both individual configurations and on average (see SM). Hence, for any given value of the disorder strength, the transmission function interpolates between a constant regime at $\omega\approx\omega_{\rm DQI}$ and the characteristic ω^2 behavior at higher energies, and the crossover scale increases with disorder strength. Above a critical threshold, the transmission function becomes qualitatively indistinguishable from that of the para configuration. Despite a lower conductance the effects of DQI are lost. This scenario emerges for both individual disorder configurations and on average. This suggests that an analysis of the conductance alone may not be conclusive for detecting DQI while the effects on the transmission function at finite energy and the corresponding non-linearity of the $I-V_b$ characteristics are more resilient to the effects of disorder (see SM).

Disorder may also be characterized by a disorder scattering length. For any given realization of static disorder the electron transport is ballistic and the transmission in the resonant regime (e.g., at the LUMO resonance) is unitary, hence $\lambda_{\rm disorder}=\infty$. After averaging over the disorder realizations the resonant transmission is reduced as [91]

$$T(\omega_{\rm LUMO})=\frac{\lambda_{\rm disorder}}{\mathcal{L}+\lambda_{\rm disorder}}. \tag{7}$$

For $\lambda_{\rm disorder}\gg\mathcal{L}$ unitary transport is restored. Taking as system size $\mathcal{L}\approx 1$ nm, estimated as the longest distance among all $\ell\to r$ channels, we find, e.g., $\lambda_{\rm disorder}\approx 1.2$ nm at $A=30$ meV, and a relation $\lambda_{\rm disorder}(A)\propto A^{-1}$ (see SM). Alternatively, if we express the condition above as

$$\frac{\lambda_{\rm disorder}}{\mathcal{L}}=\frac{T(\omega_{\rm LUMO})}{1-T(\omega_{\rm LUMO})}, \tag{8}$$

it is possible to estimate a disorder threshold (independent on $\mathcal{L}$) defined by $\lambda_{\rm disorder}\approx\mathcal{L}$, corresponding to a resonant transmission reduced to half its ballistic value. We find $A_{\rm critical}\lesssim 40$ meV, and verified that when approaching the critical disorder strength the ω^2 transmission disappears, meaning that the effects of QI are contextually lost (see SM). Experimentally, the critical value is comparable with disorder estimates for graphene on a SiO_2 substrate but well above estimates for devices encapsulated in hBN [51]. For individual disorder realizations, QI are lost only at much higher values of disorder strength (i.e., above those investigated here). We conclude that the intrinsic (i.e., static) disorder of the sample is not as detrimental to QI as averaging over several disorder configurations, which can be considered representative of a statistical analysis of the transport properties over a series of break-junction configurations.

Finally, we compare the disorder average and variance to a few energy scales relevant for electron transport, i.e., the position of the resonant ($\omega_{\rm HOMO}$ and $\omega_{\rm LUMO}$) and interference ($\omega_{\rm DQI}$) features, and the gap (Fig. 2f). Since the disorder distribution is symmetric, i.e., $\langle\epsilon_k\rangle=0$, the mean value of all quantities is close to that of the pristine sample, while their variance generally increases with disorder strength. As already discussed, the fluctuation of $\omega_{\rm DQI}$ in the individual transmission channels for each disorder realization is responsible for the enhancement of the conductance, see Figs. 2b,c,d,e. However, we also find that the gap Δ is remarkably stable against disorder, i.e., its variance is significantly lower than the variance of the frontier MOs position for any value of the disorder strength. This suggests that the dominant effect at play is rather a fluctuation of the Fermi level alignment. The data are also compatible with a weak *increase* of the gap, e.g., less than 2% with respect to the pristine value Δ_0 at $A\approx\Delta_0$.

Overall, limiting disorder to below 10 meV sufficiently limits disorder effects to still be able to observe DQI. This is readily possible for state-of-the-art substrates like hBN [90].

3.3. Electron–electron interaction

Electronic correlation arising from the Coulomb repulsion are believed to play a relevant role in electron transport, when electrons are constrained in narrow conduction channels. Unfortunately, taking into account many-body effects in the theoretical description of electron transport is a challenging task [39], and despite attempts to include dynamical correlations (in different fashions) in the recent literature [28,29,92–98], systematic studies for correlated nanoscale quantum junctions are still few and far between.

The Coulomb repulsion between π-electrons was estimated by Parr et al. [99] to be $U = 16.93\,\mathrm{eV}$, corresponding to $U/t \approx 6$. Typically, in organic molecules one should consider a Pariser–Parr–Pople model [99–101], which includes long-range interactions $V(r)$. Remarkably, Schüler et al. [102] have shown that it is possible to approximate a model with non-local interactions by an effective Hubbard model with a *screened* local interactions U. In practice, the local part of the interaction is reduced according to a weighted average of non-local interaction terms. The screened value, ranging between $U/t \approx 1.6$ for graphene and $U/t \approx 1.2$ for a benzene molecule, can supply for the missing long-range repulsion in the Hubbard model [102]. From the computational point of view, the many-body problem with non-local interactions is significantly harder than its Hubbard counterpart, and requires sophisticated techniques. In the case of benzene, numerical simulations of the Pariser–Parr–Pople model suggest that indeed non-local interactions reduce correlations effects [103], in agreement with the above screening picture. In the following, we add to the tight-binding Hamiltonian a screened local Coulomb repulsion (i.e., a Hubbard interaction) described by the Hamiltonian

$$\mathcal{H}_{e-e} = U \sum_i n_{i\uparrow} n_{i\downarrow} - \mu \sum_i (n_{i\uparrow} + n_{i\downarrow}), \tag{9}$$

where the chemical potential to be $\mu = U/2$ ensures the Fermi energy is located at $\omega = 0$ for any value of the local Coulomb repulsion. In our analysis, we take U as a parameter, which we vary within a reasonable range of values in order to explore the system behavior from the weak- to the strong-coupling regimes.

We take into account the many-body effects due to electron–electron interaction within real-space dynamical mean-field theory (DMFT). In a nutshell, each C atom is mapped onto an auxiliary impurity problem (describing a single C-pz AO) self-consistently embedded in the nanostructure, which is solved with Lánczos exact diagonalization, [104,105] similarly as in previous works [28,29,106,107]. All the many-body effects are enclosed in the electronic self-energy $\Sigma_{ij}(\omega) = \Sigma_{ii}(\omega)\delta_{ij}$, which is a diagonal matrix in the space of the carbon p_z AOs. The dynamical nature of the self-energy allows to simultaneously describe both coherent and incoherent electronic excitations living on different energy scales, giving rise to a non-trivial renormalization of the spectral features. Taking into account non-local correlations, i.e., $\Sigma_{i\neq j}(\omega)$ requires much more sophisticated and computationally expensive techniques. Numerical investigations for molecules such as benzene have shown that the dominant effect of non-local correlations is to *enhance* the HOMO-LUMO gap [103,108], whereas local correlations tend to *reduce* it instead [103,106,108,109]. Hence, in the context of the present work, it is reasonable to neglect non-local correlations, considering the (normalized) HOMO-LUMO gap Δ as a *conservative* approximation. We perform zero-temperature calculations, which can be expected to be accurate as long as thermal excitations of charge carriers across the spectral gap are negligible, i.e., for $k_B T \ll \Delta_0$, where k_B denotes Boltzmann's constant.

Real-space DMFT has been employed in the literature to describe many-body effects in a wide range of systems, lacking translational

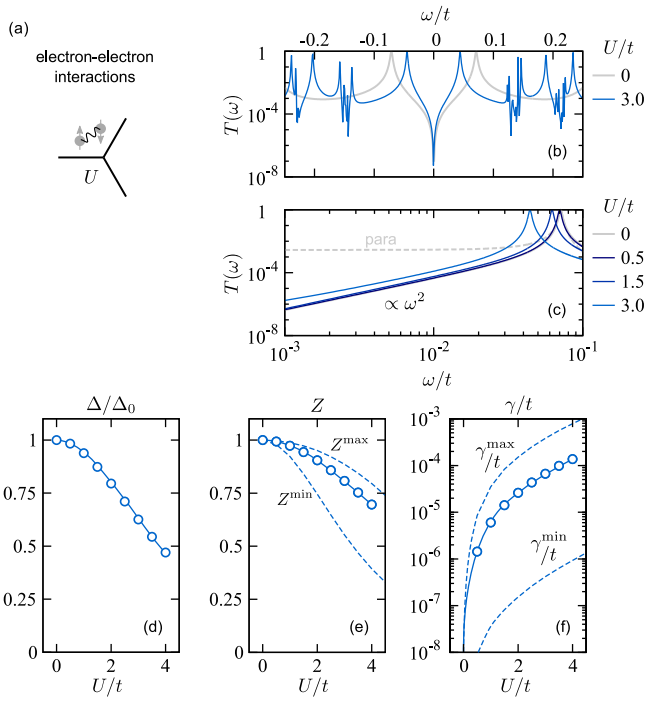

Fig. 3. (a) Schematic representation of the local Coulomb repulsion. (b) Many-body effects on the transmission function include a renormalization of the HOMO-LUMO gap, and a redistribution of spectral weight, giving rise to many-body resonances. (c) The universal behavior of the transmission function in the presence of the QI antiresonance is preserved in the presence of electron–electron interactions. (d,e,f) Evolution of the spectral gap Δ, of the average quasi-particle weight Z, and the average scattering rate γ as a function of the Coulomb repulsion U. The renormalization of the gap Δ/Δ_0 correlates with the reduction of Z and it is mostly controlled by its value at the edges $Z^{\min}$. The low scattering rate, i.e., $\gamma \ll \Gamma$, due to the lack of electronic states within the gap, cannot drive the electron transport away from the ballistic regime. (For interpretation of the references to color in this figure legend, the reader is referred to the web version of this article.)

invariance in one or more spatial directions [96–98,103,108,110–119], including graphene nanostructures [28,29,106,107,120]. To address the transport properties, the transmission function is evaluated from the Landauer formula, where the Green's function is dressed with the many-body self-energy (see also SM). In the presence of many-body correlations within the scattering region, the Landauer formula for the transmission is approximate, and vertex corrections should be taken into account. Following Ferreti et al., [121] vertex corrections to the transmission effectively renormalize the coupling

$$\Gamma^R \to \Gamma^R \left[1 + \frac{\gamma(\omega)}{\Gamma^L + \Gamma^R}\right] \tag{10}$$

where $\gamma(\omega) \propto -\Im\Sigma(\omega)$ is the scattering rate associated to electron–electron scattering and $\Gamma^{L/R} = \Gamma$ is the coupling to the leads. As long as $\gamma \ll \Gamma$, vertex corrections are negligible. As we show numerically below, this is indeed the case within the HOMO-LUMO gap Δ, where γ is strongly suppressed due to the lack of electronic states available for scattering. Hence, far from the resonant transport regime, i.e., for bias voltages $eV_b \ll \Delta$, vertex corrections can be neglected. [95,98,121–125]

In Fig. 3b,c we show how many-body effects reflect on the transmission function of the meta configuration. The primary effect is a renormalization of the HOMO-LUMO gap with respect to the tight-binding value $\Delta < \Delta_0$, see also Fig. 3d. While the low-energy structure is qualitatively identical to the one of the original tight-binding model, at higher energy scales the system displays a significantly richer electronic structure, characterized by a redistribution of spectral weight between emergent many-body resonances. Remarkably, the universal ω^2 behavior, as well as the QI antiresonance, survive in the presence

of electron–electron interactions ranging from the weak- to the strong-coupling regime [28,29]. The physics close to the Fermi energy, which is relevant for electron transport, can be rationalized – to some extent – in terms of key parameters derived from the many-body self-energy, i.e., the quasi-particle weight Z_i and scattering rate γ_i

$$Z_i = \left(1 - \frac{\partial}{\partial\omega}\Re\,\Sigma_{ii}(\omega)\Big|_{\omega=0}\right)^{-1} \tag{11}$$

$$\gamma_i = -Z_i\Im\,\Sigma_{ii}(0) \tag{12}$$

which account for the renormalization of spectral features, and the scattering rate, proportional to the (inverse) lifetime of electronic excitations, respectively. Since both depend on position and hence display some degree of spatial distribution, it is also convenient to consider their the spatial average, defined as $\mathcal{O} = n_C^{-1}\sum_i \mathcal{O}_i$ where $\mathcal{O}_i$ is a generic observable. In order to understand the behavior of those parameters as a function of the Coulomb repulsion, it is useful to recall that in the non-interactive limit ($U \to 0$) the many-body self-energy vanishes, therefore $Z \to 1$ and $\gamma \to 0$.

Within DMFT, the renormalization of the gap of a correlated insulator (or semiconductor) is controlled by the quasi-particle weight [28,29,106,109]. In a spatially-translational system, one would expect $\Delta = Z\Delta_0$. At the size considered here, the gap decreases *faster* than the average Z as a function of the Coulomb repulsion, and its behavior correlates well with the minimal value of Z over the structure ($Z^{\min}$, compare Figs. 3d,e). The lowest values of Z correspond to edge C atoms, where the balance between potential and kinetic energy tilts more towards the former compared to bulk C atoms [106,107]. The edges thus seem to control the reduction of the gap despite the average Z being closer to the bulk values, see Fig. 3e.

The many-body scattering rate γ is a measure of the dampening of the electronic excitations at the Fermi energy, while at finite energy, the self-energy induces broadening of the spectral and transport features. In a semiconductor (or insulator) the scattering rate is dramatically suppressed due to the lack of electronic states available for the scattering. As show in Fig. 3f, γ increases with the Coulomb repulsion, yet only becomes comparable with the interface scattering to the leads (i.e., $\gamma \sim \Gamma$) towards the strong-coupling regime. In this scenario, the scattering time $\tau_{e-e} = \hbar/\gamma \approx 100\,\mathrm{fs}$ suggests that long-lived electronic excitations propagate through the graphene nanostructure. Assuming a typical value $v_F \approx 1\times10^6\,\mathrm{m\,s^{-1}}$ for the Fermi velocity in free-standing graphene [126], the electron–electron scattering length can be estimated as $\lambda_{e-e} = v_F\tau_{e-e} \approx 100\,\mathrm{nm}$, which is significantly longer than the size of the nanostructures considered here. This scenario is in stark contrast with Mott insulators, where the electronic excitation within the (correlated) energy gap features an extremely short lifetime [127,128] and molecules in a open-shell configuration [129].

Hence, the primary effect of electronic-electron scattering is a renormalization of the spectral gap, while the electronic transport mechanism is dominated by coherent quasi-particles, and a QI antiresonance is clearly observed also in the presence of a strong Coulomb repulsion.

Finally, it is worth mentioning that graphene nanostructures with zig-zag edges are prone towards magnetism. If the Coulomb interaction is strong enough, the magnetic ground state is a global singlet with an antiferromagnetic (Néel) real-space pattern [83,106,130]. In this state, the chiral and magnetic sublattices coincide, so that in the meta configuration, the $\{\ell\}$ and $\{r\}$ contact atoms have the same spin polarization. Remarkably, QI effects survive also in the magnetic state, and the DQI antiresonances in two spin channels appear at different energies, i.e., $\omega_\uparrow^{\mathrm{DQI}}$ and $\omega_\downarrow^{\mathrm{DQI}}$, yielding a strong spin polarization of the transmission function [28,29,120]. This effect was suggested as a novel mechanism, e.g., to realize a spin filter operating on QI [28] and for spin-caloritronic applications [120].

3.4. Electron–phonon interaction

Molecular vibrations are another possible source of scattering for electrons. In the literature, a strong inelastic vibrational signal has been reported close to electron transmission resonances through graphene nanoconstrictions [131], and the phonon-induced dephasing has been suggested to be most relevant for molecular junctions in the meta configuration [71]. Indeed, evidence of a partial quenching of DQI in molecular junctions due to inelastic electron–phonon contributions has been reported both theoretically [94] and experimentally [41,132]. However, QI effects are not completely destroyed, not even at room temperature, as the conductance difference between junction in the meta and para configurations still remains substantial [94].

In the following, we analyze the effects of electron–phonon scattering on the electronic transmission through small graphene nanoflakes. Given the comparatively small sample size (compared to large-scale graphene devices) we are interested in coupling through bosonic vibrational modes rather than long-wavelength acoustic phonons [133,134]. For the sake of simplicity, we consider the coupling to a dispersionless such mode, so that the coupled electron–phonon system is described by the Fröhlich Hamiltonian

$$\mathcal{H}_{\mathrm{Fröhlich}} = \mathcal{H}_0 + \mathcal{H}_{\mathrm{ph}} + \mathcal{H}_{\mathrm{e-ph}} \tag{13}$$

with

$$\mathcal{H}_{\mathrm{ph}} = \omega_{ph}\left(a^\dagger a + \frac{1}{2}\right) \tag{14}$$

and

$$\mathcal{H}_{\mathrm{e-ph}} = (a^\dagger g^* + a g)\sum_{i\sigma} n_{i\sigma}, \tag{15}$$

where a ($a^\dagger$) is the bosonic annihilation (creation) operator of a phonon with energy ω_{ph}, coupled to the local electron density n_i through a complex electron–phonon coupling matrix which is diagonal in the phonon subspace, $g = |g|\exp(\imath\phi)$, where ϕ is a random phase. We treat both ω_{ph} and g as parameters, in order to understand the effect of electron–phonon scattering on the QI features in different regimes. For coupling to vibrational modes, prefactors $g = \lambda\omega_{ph}$ with $\lambda \approx 0.7$ have been estimated [134], corresponding to $g \approx 20\,\mathrm{meV}$, i.e., at the lower end of the values we investigate here. Typical values of the electron–phonon coupling for graphene on a substrate have been estimated to be 38 meV on SiO_2 and 62 meV on hBN [135].

The expanded Hilbert space we simulate is spanned by a direct product of the electronic and phononic degrees of freedom, i.e., $n_C\cdot n_{ph}$, with n_{ph} the number of phononic excitations. We compute the transmission $T_{0\to n}(\omega;\omega_{ph})$ with a fixed ω_{ph}, from an incoming mode with $n = 0$ phonons to each outgoing mode with $-n_{ph} \le n \le n_{ph}$ phonons. These contributions are added fully coherently by taking the trace in the Landauer formula over the phononic degrees of freedom. We also sample the phase ϕ of the electron–phonon coupling, in order to get the total transmission $T(\omega;\omega_{ph})$. We further extend our analysis from a single- to a multi-mode scenario by incoherently superimposing transmission functions $T(\omega;\omega_{ph})$ over a range of phonon frequencies, weighted with a Boltzmann factor evaluated at $T = 300\,\mathrm{K}$ (i.e., $k_BT \approx 26\,\mathrm{meV}$) that takes into account the thermal occupation of the corresponding phonon mode (for a step-by-step description of all procedures see SM). Within this approximation, we neglect higher-order processes such as multiple, coherent scattering of phonons between several electrons. Treating such effects would require a Keldysh Green's function formalism with an explicit simultaneous treatment of all electrons within the considered bias window. Given the comparatively small electron–phonon (or electron–vibron) coupling, and the limited size of our scattering region, neglecting the coherence between multiple scattering events seems like a valid approximation, at least for bias voltages not substantially exceeding the energy of the considered vibrational modes.

We calculate the transmission function for different values of the electron–phonon coupling g. In the single-mode approximation

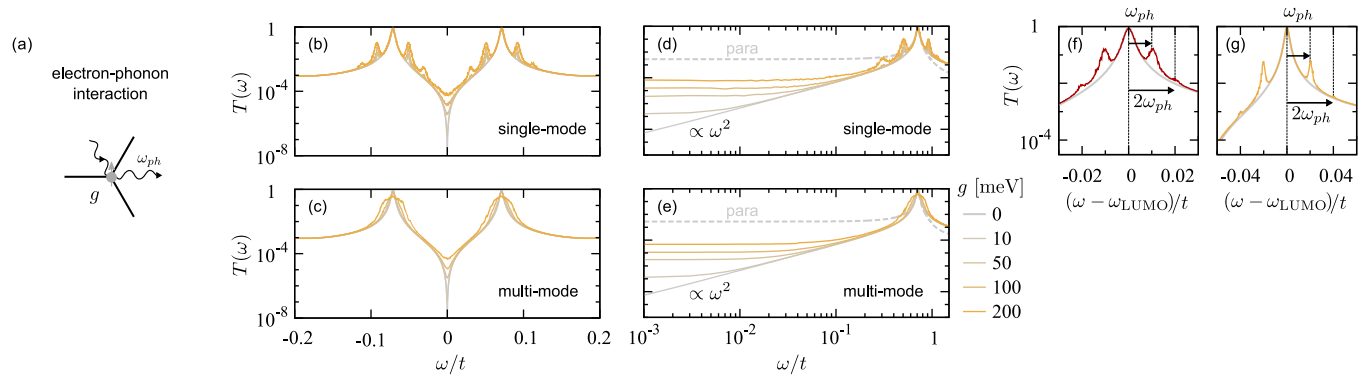

Fig. 4. (a) Schematic representation of the electron–phonon interaction. (b,c) Effects of the electron–phonon coupling on the transmission function. In the single-mode case, phonon satellite peaks are visible at integer multiples of $\omega_{ph} = 26\,\mathrm{meV}$ around the frontier MOs. In the multi-mode case, the weighted average over ω_{ph} at 300 K broadens the resonances, and the transmission at the frontier MOs is no longer unitary. (d,e) Evolution of the universal behavior of the transmission function across the weak- to the strong-electron–phonon coupling regimes. The transmission functions of the corresponding pristine para configurations is also given as a reference (dashed gray lines). (f,g) Single-mode transmission function around ω_{LUMO} for $\omega_{ph} = 13\,\mathrm{meV}$ (red line) and $\omega_{ph} = 26\,\mathrm{meV}$ (orange line) and $g = 100\,\mathrm{meV}$ compared to the result for $g = 0$ (gray line). The arrows and the dashed lines highlight the phonon satellite peaks. (For interpretation of the references to color in this figure legend, the reader is referred to the web version of this article.)

(Figs. 4b,d), we observe phonon satellite peaks around the frontier MO resonances, at integer multiples of the phonon frequency (Figs. 4f,g) for different values of ω_{ph}. Focusing on the transmission function close to the antiresonance, we find that it is enhanced quadratically with the electron–phonon coupling, i.e., $T(\omega_{\mathrm{DQI}}) \propto g^2$, in close analogy to the effect of disorder. Continuing the analogy, we also observe that for a given value of the electron–phonon coupling, the transmission function interpolates between a constant regime at $\omega \approx \omega_{\mathrm{DQI}}$ and the characteristic ω^2 behavior at higher energies. The crossover scale again increases with the electron–phonon coupling. Above a critical threshold, the transmission function becomes qualitatively indistinguishable from that of the para configuration. In the multi-mode case, instead of generating individual phonon satellites, the electron–phonon coupling broadens the resonances so that electron transport through the MOs is no longer unitary as shown in Figs. 4c,e. The effects on the antiresonance are qualitatively similar to those observed in the single-mode scenario. The transmission in the single-mode scenario features fewer, more pronounced peaks than the multi-mode version, where the superposition of satellite peaks at different energies results in a broadening of the resonance. While the position of the DQI antiresonance is not affected by the electron–phonon interaction, the transmission probability at $\omega \approx \omega_{\mathrm{DQI}}$ increases due to contributions of scattering channels involving phononic excitations. The dichotomy between the effects close to the antiresonance and at higher energy scales appears to be a generic feature of the suppression of QI, which applies to different scattering mechanisms.

Since in our numerical framework, the electronic subsystem is no longer energy-conserving, nor do we define an electronic self-energy, we cannot estimate a scattering length as we did in the case of disorder or electron–electron interactions. Therefore, we employ an alternative strategy that allows us to estimate the inelastic scattering length as a function of the electron–phonon coupling. In a nutshell, we consider the probability distribution of $T_{0\to n}(\omega = 0; \omega_{ph})$ as a random walk in n. As the number of steps increases, we can fit a Gaussian distribution with width proportional to $\lambda_{\mathrm{e-ph}}/\mathcal{L}$ (the detailed procedure is described in the SM). For instance, we find $\lambda_{\mathrm{e-ph}} \approx 10\,\mathrm{nm}$ at $g = 20\,\mathrm{meV}$ but we only reach the typical system size $\lambda_{\mathrm{e-ph}} \approx 2\,\mathrm{nm}$ at $g = 100\,\mathrm{meV}$. Following a random walk argument in the space of possible bosonic excitations, we obtain a relation $\lambda_{\mathrm{e-ph}}(g) \propto g^{-1}$ (see SM), analogous to the case of disorder. Upon comparison with the numerical data for the transmission function, this corresponds to the coupling range in which the characteristic ω^2 behavior of the meta configuration is no longer observable and hence the effects of QI are contextually lost.

In summary, phonons (or, more generally, inelastic scattering) limit DQI effects as soon as $k_B T$ exceeds the size of the HOMO-LUMO gap, in line with a much more simple estimate of smearing out the conductance on this energy scale. We, therefore, conclude that explicit consideration of electron–phonon scattering does not pose an additional limit to the observability of DQI.

4. Discussion and conclusions

The focus of the present work is the resilience of QI effects in the electron transport through graphene nanostructures. In the ballistic transport regime, the stability of DQI is rooted in its topological and symmetry origin, as also established in the recent literature. Furthermore, we investigated several effects, which can be possibly detrimental to QI, and for each we estimate a characteristic scale above which QI effects are likely to be lost.

Our findings can be summarized as follows. (i) A size effects analysis reveals that in the ballistic regime, the in-gap transmission function displays a characteristic ω^2 behavior that can be entirely ascribed to the presence of a QI antiresonance. In this regime, the transmission function is a universal function of the ratio between the molecule-lead coupling and the width of the gap, i.e., Γ/Δ_0. In turn, it also determines an intrinsic resolution threshold necessary to resolve QI effects. (ii) The dominant effect of local many-body correlations due to the Coulomb repulsion is to renormalize the gap $\Delta < \Delta_0$ and, as long as thermal excitations of electrons across the gap are negligible, the electron–electron scattering rate is low and the effect on the QI properties is marginal. (iii) For disorder and electron–phonon scattering, we identify a similar behavior of the transmission function. Close to the antiresonance the transmission function is strongly enhanced with analogous scaling laws versus disorder strength A and electron–phonon coupling g, whereas at higher energies the characteristic ω^2 behavior is more resilient. For typical values reported in the literature, QI can be suppressed for graphene devices deposited on substrates like SiO_2 but not for cleaner devices deposited on hBN. The electron–phonon coupling in graphene (as well as in organic molecules) is typically low-enough that even at room temperature QI effects can survive.

While we investigated each case independently, multiple scattering sources are simultaneously in play. Hence, the effective electron lifetime is dominated by the process with the highest scattering rate (i.e., with the lowest lifetime or scattering length). Specifically, the overall scattering time is determined like a resistance in parallel

$$\frac{1}{\tau} = \frac{1}{\tau_\Gamma} + \frac{1}{\tau_{\mathrm{disorder}}} + \frac{1}{\tau_{\mathrm{e-e}}} + \frac{1}{\tau_{\mathrm{e-ph}}} + \cdots, \tag{16}$$

where the characteristic times correspond to processes involving electron scattering at the interface with the leads τ_Γ, off disorder (τ_{disorder}),

off other electronic (τ_{e-e}) and phononic (τ_{e-ph}) excitations, respectively, and similarly for any other possible process not explicitly included here.

Within the present framework some effects can be combined with some additional effort, e.g., disorder with either electron–electron or electron–phonon interactions. For instance, we speculate that in the presence of the electronic correlations, the disorder-driven Fermi level alignment fluctuations could be reduced, especially for weak-to-moderate disorder $|\epsilon_i| \ll U$. The argument is that the Coulomb repulsion penalizes a spatially inhomogeneous charge distribution, [106,107] and is expected to compete with disorder by renormalizing the disorder potential, i.e., $\epsilon_i \to \epsilon_i + \Re\Sigma_{ii}(0)$. Other combinations, such as the simultaneous treatment of electron–electron and electron–phonon interactions are very challenging, and are beyond the scope of the present analysis.

In conclusion, our analysis provides a unified theoretical ground to explore the resilience of QI effects, and the necessary conditions for observing them under experimental conditions. At the same time, the conductance alone may be insufficient for a characterization of the QI properties of a junction, while identifying non-linear $I - V_b$ characteristics can reveal the presence of an antiresonance even when partially concealed or suppressed due to the Fermi level alignment or electronic scattering.

CRediT authorship contribution statement

Angelo Valli: Conceptualization, Methodology, Software, Investigation, Writing – original draft, Writing – review & editing, Visualization, Supervision, Funding acquisition. **Thomas Fabian:** Software, Investigation, Writing – original draft, Writing – review & editing. **Florian Libisch:** Conceptualization, Methodology, Software, Investigation, Resources, Writing – original draft, Writing – review & editing, Funding acquisition. **Robert Stadler:** Conceptualization, Methodology, Resources, Writing – original draft, Writing – review & editing, Supervision, Funding acquisition.

Declaration of competing interest

The authors declare that they have no known competing financial interests or personal relationships that could have appeared to influence the work reported in this paper.

Acknowledgments

We are thankful to A. Amaricci and M. Capone for helpful discussion and for providing the Lánczos impurity solver [104,105]. We acknowledges financial support from the Austrian Science Fund (FWF) project number No. P31631 (AV and RS). TF and FL acknowledge support from FWF, Austria (DACH proposal I3827-N36) and WWTF, Austria project MA14-002. Preliminary work for this project was also supported through the FWF Erwin Schrödinger, Austria fellowship J3890-N36 (AV).

Appendix A. Supplementary data

Supplementary material related to this article can be found online at https://doi.org/10.1016/j.carbon.2023.118358.

References

[1] C.M. Guédon, H. Valkenier, T. Markussen, K.S. Thygesen, J.C. Hummelen, S.J. van der Molen, Observation of quantum interference in molecular charge transport, Nature Nanotechnol. 7 (5) (2012) 305–309, http://dx.doi.org/10.1038/nnano.2012.37.

[2] R. Frisenda, V.A.E.C. Janssen, F.C. Grozema, H.S.J. van der Zant, N. Renaud, Mechanically controlled quantum interference in individual π-stacked dimers, Nature Chem. 8 (12) (2016) 1099–1104, http://dx.doi.org/10.1038/nchem.2588.

[3] Z. Chen, L. Chen, G. Li, Y. Chen, C. Tang, L. Zhang, J. Liu, L. Chen, Y. Yang, J. Shi, J. Liu, H. Xia, W. Hong, Control of quantum interference in single-molecule junctions via jahn-teller distortion, Cell Rep. Phys. Sci. 2 (2) (2021) 100329, http://dx.doi.org/10.1016/j.xcrp.2021.100329.

[4] H. Chen, Y. Chen, H. Zhang, W. Cao, C. Fang, Y. Zhou, Z. Xiao, J. Shi, W. Chen, J. Liu, W. Hong, Quantum interference enhanced thermopower in single-molecule thiophene junctions, Chin. Chem. Lett. 33 (1) (2022) 523–526, http://dx.doi.org/10.1016/j.cclet.2021.06.052.

[5] J.E. Greenwald, J. Cameron, N.J. Findlay, T. Fu, S. Gunasekaran, P.J. Skabara, L. Venkataraman, Highly nonlinear transport across single-molecule junctions via destructive quantum interference, Nature Nanotechnol. 16 (3) (2020) 313–317, http://dx.doi.org/10.1038/s41565-020-00807-x.

[6] J. Bai, A. Daaoub, S. Sangtarash, X. Li, Y. Tang, Q. Zou, H. Sadeghi, S. Liu, X. Huang, Z. Tan, J. Liu, Y. Yang, J. Shi, G. Mészáros, W. Chen, C. Lambert, W. Hong, Anti-resonance features of destructive quantum interference in single-molecule thiophene junctions achieved by electrochemical gating, Nature Mater. 18 (4) (2019) 364–369, http://dx.doi.org/10.1038/s41563-018-0265-4.

[7] H. Vazquez, R. Skouta, S. Schneebeli, M. Kamenetska, R. Breslow, L. Venkataraman, M. Hybertsen, Probing the conductance superposition law in single-molecule circuits with parallel paths, Nature Nanotechnol. 7 (10) (2012) 663–667, http://dx.doi.org/10.1038/nnano.2012.147.

[8] J. Hurtado-Gallego, S. Sangtarash, R. Davidson, L. Rincón-García, A. Daaoub, G. Rubio-Bollinger, C.J. Lambert, V.S. Oganesyan, M.R. Bryce, N. Agraït, H. Sadeghi, Thermoelectric enhancement in single organic radical molecules, Nano Lett. 22 (3) (2022) 948–953, http://dx.doi.org/10.1021/acs.nanolett.1c03698.

[9] X. Wang, T.L.R. Bennett, A. Ismael, L.A. Wilkinson, J. Hamill, A.J.P. White, I.M. Grace, O.V. Kolosov, T. Albrecht, B.J. Robinson, N.J. Long, L.F. Cohen, C.J. Lambert, Scale-up of room-temperature constructive quantum interference from single molecules to self-assembled molecular-electronic films, J. Am. Chem. Soc. 142 (19) (2020) 8555–8560, http://dx.doi.org/10.1021/jacs.9b13578.

[10] S.V. Aradhya, L. Venkataraman, Single-molecule junctions beyond electronic transport, Nature Nanotechnol. 8 (6) (2013) 399–410, http://dx.doi.org/10.1038/nnano.2013.91.

[11] C. Tang, L. Huang, S. Sangtarash, M. Noori, H. Sadeghi, H. Xia, W. Hong, Reversible switching between destructive and constructive quantum interference using atomically precise chemical gating of single-molecule junctions, J. Am. Chem. Soc. 143 (25) (2021) 9385–9392, http://dx.doi.org/10.1021/jacs.1c00928.

[12] D. Nozaki, S.M. Avdoshenko, H. Sevinçli, R. Gutierrez, G. Cuniberti, Prediction of quantum interference in molecular junctions using a parabolic diagram: Understanding the origin of Fano and anti- resonances, J. Phys. Conf. Ser. 427 (2013) 012013, http://dx.doi.org/10.1088/1742-6596/427/1/012013.

[13] C.J. Lambert, Basic concepts of quantum interference and electron transport in single-molecule electronics, Chem. Soc. Rev. 44 (4) (2015) 875–888, http://dx.doi.org/10.1039/c4cs00203b.

[14] Y. Geng, S. Sangtarash, C. Huang, H. Sadeghi, Y. Fu, W. Hong, T. Wandlowski, S. Decurtins, C.J. Lambert, S.-X. Liu, Magic ratios for connectivity-driven electrical conductance of graphene-like molecules, J. Am. Chem. Soc. 137 (13) (2015) 4469–4476, http://dx.doi.org/10.1021/jacs.5b00335.

[15] S. Sangtarash, C. Huang, H. Sadeghi, G. Sorohhov, J. Hauser, T. Wandlowski, W. Hong, S. Decurtins, S.-X. Liu, C.J. Lambert, Searching the hearts of graphene-like molecules for simplicity, sensitivity, and logic, J. Am. Chem. Soc. 137 (35) (2015) 11425–11431, http://dx.doi.org/10.1021/jacs.5b06558.

[16] S. Sangtarash, H. Sadeghi, C.J. Lambert, Exploring quantum interference in heteroatom-substituted graphene-like molecules, Nanoscale 8 (27) (2016) 13199–13205, http://dx.doi.org/10.1039/c6nr01907b.

[17] T. Hansen, G.C. Solomon, When conductance is less than the sum of its parts: Exploring interference in multiconnected molecules, J. Phys. Chem. C 120 (12) (2016) 6295–6301, http://dx.doi.org/10.1021/acs.jpcc.5b11211.

[18] D.Z. Manrique, C. Huang, M. Baghernejad, X. Zhao, O.A. Al-Owaedi, H. Sadeghi, V. Kaliginedi, W. Hong, M. Gulcur, T. Wandlowski, M.R. Bryce, C.J. Lambert, A quantum circuit rule for interference effects in single-molecule electrical junctions, Nature Commun. 6 (1) (2015) http://dx.doi.org/10.1038/ncomms7389.

[19] P. Gehring, H. Sadeghi, S. Sangtarash, C.S. Lau, J. Liu, A. Ardavan, J.H. Warner, C.J. Lambert, G.A.D. Briggs, J.A. Mol, Quantum interference in graphene nanoconstrictions, Nano Lett. 16 (7) (2016) 4210–4216, http://dx.doi.org/10.1021/acs.nanolett.6b01104.

[20] H. Sadeghi, J.A. Mol, C.S. Lau, G.A.D. Briggs, J. Warner, C.J. Lambert, Conductance enlargement in picoscale electroburnt graphene nanojunctions, Proc. Natl. Acad. Sci. 112 (9) (2015) 2658–2663, http://dx.doi.org/10.1073/pnas.1418632112.

[21] X.-L. Wei, Y.-P. Chen, W.-L. Liu, J.-X. Zhong, Enhanced gas sensor based on nitrogen-vacancy graphene nanoribbons, Phys. Lett. A 376 (4) (2012) 559–562, http://dx.doi.org/10.1016/j.physleta.2011.10.055.

[22] W. Qiu, P. Nguyen, E. Skafidas, Graphene nanopores: Electronic transport properties and design methodology, Phys. Chem. Chem. Phys. 16 (4) (2014) 1451–1459, http://dx.doi.org/10.1039/c3cp53777c.

[23] R. Stadler, S. Ami, C. Joachim, M. Forshaw, Integrating logic functions inside a single molecule, Nanotechnology 15 (4) (2004) S115–S121, http://dx.doi.org/10.1088/0957-4484/15/4/001.

[24] D.M. Cardamone, C.A. Stafford, S. Mazumdar, Controlling quantum transport through a single molecule, Nano Lett. 6 (11) (2006) 2422–2426, http://dx.doi.org/10.1021/nl0608442.

[25] C.A. Stafford, D.M. Cardamone, S. Mazumdar, The quantum interference effect transistor, Nanotechnology 18 (42) (2007) 424014, http://dx.doi.org/10.1088/0957-4484/18/42/424014.

[26] A. Daaoub, S. Sangtarash, H. Sadeghi, Switching quantum interference in phenoxyquinone single molecule junction with light, Nanomaterials 10 (8) (2020) 1544, http://dx.doi.org/10.3390/nano10081544.

[27] M.B. Lundeberg, J.A. Folk, Spin-resolved quantum interference in graphene, Nat. Phys. 5 (12) (2009) 894–897, http://dx.doi.org/10.1038/nphys1421.

[28] A. Valli, A. Amaricci, V. Brosco, M. Capone, Quantum interference assisted spin filtering in graphene nanoflakes, Nano Lett. 18 (3) (2018) 2158–2164, http://dx.doi.org/10.1021/acs.nanolett.8b00453.

[29] A. Valli, A. Amaricci, V. Brosco, M. Capone, Interplay between destructive quantum interference and symmetry-breaking phenomena in graphene quantum junctions, Phys. Rev. B 100 (2019) 075118, http://dx.doi.org/10.1103/PhysRevB.100.075118, URL https://link.aps.org/doi/10.1103/PhysRevB.100.075118.

[30] A.N. Pal, D. Li, S. Sarkar, S. Chakrabarti, A. Vilan, L. Kronik, A. Smogunov, O. Tal, Nonmagnetic single-molecule spin-filter based on quantum interference, Nature Commun. 10 (1) (2019) http://dx.doi.org/10.1038/s41467-019-13537-z.

[31] X.-H. Cao, D. Wu, Y.-X. Feng, W.-X. Zhou, L.-M. Tang, K.-Q. Chen, Effect of electrophilic substitution and destructive quantum interference on the thermoelectric performance in molecular devices, J. Phys.: Condens. Matter 31 (34) (2019) 345303, http://dx.doi.org/10.1088/1361-648x/ab2299.

[32] R. Almughathawi, S. Hou, Q. Wu, Z. Liu, W. Hong, C. Lambert, Conformation and quantum-interference-enhanced thermoelectric properties of diphenyl diketopyrrolopyrrole derivatives, ACS Sens. 6 (2) (2020) 470–476, http://dx.doi.org/10.1021/acssensors.0c02043.

[33] J. Prasongkit, A.R. Rocha, Quantum interference effects in biphenyl dithiol for gas detection, RSC Adv. 6 (64) (2016) 59299–59304, http://dx.doi.org/10.1039/c6ra06578c.

[34] O. Sengul, J. Völkle, A. Valli, R. Stadler, Enhancing the sensitivity and selectivity of pyrene-based sensors for detection of small gaseous molecules via destructive quantum interference, Phys. Rev. B 105 (2022) 165428, http://dx.doi.org/10.1103/PhysRevB.105.165428, URL https://link.aps.org/doi/10.1103/PhysRevB.105.165428.

[35] M. Brack, R. Bhaduri, Semiclassical Physics, CRC Press, Boca Raton, FL, 2003.

[36] X. Zhao, V. Geskin, R. Stadler, Destructive quantum interference in electron transport: A reconciliation of the molecular orbital and the atomic orbital perspective, J. Chem. Phys. 146 (9) (2017) 092308, http://dx.doi.org/10.1063/1.4972572.

[37] S. Gunasekaran, J.E. Greenwald, L. Venkataraman, Visualizing quantum interference in molecular junctions, Nano Lett. 20 (4) (2020) 2843–2848, http://dx.doi.org/10.1021/acs.nanolett.0c00605.

[38] D. Fracasso, H. Valkenier, J.C. Hummelen, G.C. Solomon, R.C. Chiechi, Evidence for quantum interference in SAMs of arylethynylene thiolates in tunneling junctions with eutectic Ga–In (EGaIn) top-contacts, J. Am. Chem. Soc. 133 (24) (2011) 9556–9563, http://dx.doi.org/10.1021/ja202471m.

[39] F. Evers, R. Korytár, S. Tewari, J.M. van Ruitenbeek, Advances and challenges in single-molecule electron transport, Rev. Modern Phys. 92 (2020) 035001, http://dx.doi.org/10.1103/RevModPhys.92.035001, URL https://link.aps.org/doi/10.1103/RevModPhys.92.035001.

[40] Y. Zhang, G. Ye, S. Soni, X. Qiu, T.L. Krijger, H.T. Jonkman, M. Carlotti, E. Sauter, M. Zharnikov, R.C. Chiechi, Controlling destructive quantum interference in tunneling junctions comprising self-assembled monolayers via bond topology and functional groups, Chem. Sci. 9 (19) (2018) 4414–4423, http://dx.doi.org/10.1039/c8sc00165k.

[41] C. Bessis, M.L.D. Rocca, C. Barraud, P. Martin, J.C. Lacroix, T. Markussen, P. Lafarge, Probing electron-phonon excitations in molecular junctions by quantum interference, Sci. Rep. 6 (1) (2016) http://dx.doi.org/10.1038/srep20899.

[42] L. Wang, Z. Zhao, D.B. Shinde, Z. Lai, D. Wang, Modulation of destructive quantum interference by bridge groups in truxene-based single-molecule junctions, Chem. Commun. 57 (5) (2021) 667–670, http://dx.doi.org/10.1039/d0cc07438a.

[43] C.R. Arroyo, R. Frisenda, K. Moth-Poulsen, J.S. Seldenthuis, T. Bjørnholm, H.S. van der Zant, Quantum interference effects at room temperature in OPV-based single-molecule junctions, Nanoscale Res. Let. 8 (1) (2013) http://dx.doi.org/10.1186/1556-276x-8-234.

[44] S. Richert, J. Cremers, I. Kuprov, M.D. Peeks, H.L. Anderson, C.R. Timmel, Constructive quantum interference in a bis-copper six-porphyrin nanoring, Nature Commun. 8 (2017) 14842, http://dx.doi.org/10.1038/ncomms14842.

[45] G. Calogero, I. Alcón, N. Papior, A.-P. Jauho, M. Brandbyge, Quantum interference engineering of nanoporous graphene for carbon nanocircuitry, J. Am. Chem. Soc. 141 (33) (2019) 13081–13088, http://dx.doi.org/10.1021/jacs.9b04649.

[46] S. Caneva, P. Gehring, V.M. García-Suárez, A. García-Fuente, D. Stefani, I.J. Olavarria-Contreras, J. Ferrer, C. Dekker, H.S.J. van der Zant, Mechanically controlled quantum interference in graphene break junctions, Nature Nanotechnol. 13 (12) (2018) 1126–1131, http://dx.doi.org/10.1038/s41565-018-0258-0.

[47] S. Sato, Graphene for nanoelectronics, Japan. J. Appl. Phys. 54 (4) (2015) 040102, http://dx.doi.org/10.7567/jjap.54.040102.

[48] J. Cai, P. Ruffieux, R. Jaafar, M. Bieri, T. Braun, S. Blankenburg, M. Muoth, A.P. Seitsonen, M. Saleh, X. Feng, K. Müllen, R. Fasel, Atomically precise bottom-up fabrication of graphene nanoribbons, Nature 466 (7305) (2010) 470–473, http://dx.doi.org/10.1038/nature09211.

[49] M.H.D. Guimarães, H. Gao, Y. Han, K. Kang, S. Xie, C.-J. Kim, D.A. Muller, D.C. Ralph, J. Park, Atomically thin ohmic edge contacts between two-dimensional materials, ACS Nano 10 (6) (2016) 6392–6399, http://dx.doi.org/10.1021/acsnano.6b02879.

[50] L. Wang, I. Meric, P.Y. Huang, Q. Gao, Y. Gao, H. Tran, T. Taniguchi, K. Watanabe, L.M. Campos, D.A. Muller, J. Guo, P. Kim, J. Hone, K.L. Shepard, C.R. Dean, One-dimensional electrical contact to a two-dimensional material, Science 342 (6158) (2013) 614–617, http://dx.doi.org/10.1126/science.1244358.

[51] D. Rhodes, S.H. Chae, R. Ribeiro-Palau, J. Hone, Disorder in van der Waals heterostructures of 2D materials, Nature Mater. 18 (6) (2019) 541–549, http://dx.doi.org/10.1038/s41563-019-0366-8.

[52] T.C. Li, S.-P. Lu, Quantum conductance of graphene nanoribbons with edge defects, Phys. Rev. B 77 (2008) 085408, http://dx.doi.org/10.1103/PhysRevB.77.085408, URL https://link.aps.org/doi/10.1103/PhysRevB.77.085408.

[53] H. Yin, W. Li, X. Hu, R. Tao, Coherent transport of armchair graphene constrictions, J. Appl. Phys. 107 (10) (2010) 103706, http://dx.doi.org/10.1063/1.3391273.

[54] K. Wakabayashi, M. Sigrist, Zero-conductance resonances due to flux states in nanographite ribbon junctions, Phys. Rev. Lett. 84 (2000) 3390–3393, http://dx.doi.org/10.1103/PhysRevLett.84.3390, URL https://link.aps.org/doi/10.1103/PhysRevLett.84.3390.

[55] P. Darancet, V. Olevano, D. Mayou, Coherent electronic transport through graphene constrictions: Subwavelength regime and optical analogy, Phys. Rev. Lett. 102 (2009) 136803, http://dx.doi.org/10.1103/PhysRevLett.102.136803, URL https://link.aps.org/doi/10.1103/PhysRevLett.102.136803.

[56] D. Gunlycke, C.T. White, Graphene interferometer, Appl. Phys. Lett. 93 (12) (2008) 122106, http://dx.doi.org/10.1063/1.2988825.

[57] M. Niţă, M. Ţolea, B. Ostahie, Transmission phase lapses at zero energy in graphene quantum dots, Phys. Status Solidi (RRL) - Rap. Res. Lett. 08 (09) (2014) 790–793, http://dx.doi.org/10.1002/pssr.201409228.

[58] M. Niţă, M. Ţolea, D.C. Marinescu, Robust conductance zeros in graphene quantum dots and other bipartite systems, Phys. Rev. B 101 (2020) 235318, http://dx.doi.org/10.1103/PhysRevB.101.235318, URL https://link.aps.org/doi/10.1103/PhysRevB.101.235318.

[59] G.M. Rutter, J.N. Crain, N.P. Guisinger, T. Li, P.N. First, J.A. Stroscio, Scattering and interference in epitaxial graphene, Science 317 (5835) (2007) 219–222, http://dx.doi.org/10.1126/science.1142882.

[60] H. Yang, A.J. Mayne, M. Boucherit, G. Comtet, G. Dujardin, Y. Kuk, Quantum interference channeling at graphene edges, Nano Lett. 10 (3) (2010) 943–947, http://dx.doi.org/10.1021/nl9038778.

[61] M. Oksanen, A. Uppstu, A. Laitinen, D.J. Cox, M.F. Craciun, S. Russo, A. Harju, P. Hakonen, Single-mode and multimode Fabry-Pérot interference in suspended graphene, Phys. Rev. B 89 (2014) 121414, http://dx.doi.org/10.1103/PhysRevB.89.121414, URL https://link.aps.org/doi/10.1103/PhysRevB.89.121414.

[62] D. Bischoff, F. Libisch, J. Burgdörfer, T. Ihn, K. Ensslin, Characterizing wave functions in graphene nanodevices: Electronic transport through ultrashort graphene constrictions on a boron nitride substrate, Phys. Rev. B 90 (2014) 115405, http://dx.doi.org/10.1103/PhysRevB.90.115405, URL https://link.aps.org/doi/10.1103/PhysRevB.90.115405.

[63] F. Giannazzo, S. Sonde, R.L. Nigro, E. Rimini, V. Raineri, Mapping the density of scattering centers limiting the electron mean free path in graphene, Nano Lett. 11 (11) (2011) 4612–4618, http://dx.doi.org/10.1021/nl2020922.

[64] T. Markussen, R. Stadler, K.S. Thygesen, The relation between structure and quantum interference in single molecule junctions, Nano Lett. 10 (10) (2010) 4260–4265, http://dx.doi.org/10.1021/nl101688a.

[65] T. Markussen, R. Stadler, K.S. Thygesen, Graphical prediction of quantum interference-induced transmission nodes in functionalized organic molecules, Phys. Chem. Chem. Phys. 13 (32) (2011) 14311, http://dx.doi.org/10.1039/c1cp20924h.

[66] K.G.L. Pedersen, A. Borges, P. Hedegård, G.C. Solomon, M. Strange, Illusory connection between cross-conjugation and quantum interference, J. Phys. Chem. C 119 (48) (2015) 26919–26924, http://dx.doi.org/10.1021/acs.jpcc.5b10407.

[67] R. Stadler, Comment on "breakdown of interference rules in Azulene, a nonalternant hydrocarbon", Nano Lett. 15 (11) (2015) 7175–7176, http://dx.doi.org/10.1021/acs.nanolett.5b03468.

[68] T. Stuyver, S. Fias, F.D. Proft, P. Geerlings, Back of the envelope selection rule for molecular transmission: A curly arrow approach, J. Phys. Chem. C 119 (47) (2015) 26390–26400, http://dx.doi.org/10.1021/acs.jpcc.5b10395.

[69] L.J. O'Driscoll, M.R. Bryce, Extended curly arrow rules to rationalise and predict structural effects on quantum interference in molecular junctions, Nanoscale 13 (2) (2021) 1103–1123, http://dx.doi.org/10.1039/d0nr07819k.

[70] C.A. Coulson, G.S. Rushbrooke, Note on the method of molecular orbitals, Math. Proc. Camb. Phil. Soc. 36 (2) (1940) 193–200, http://dx.doi.org/10.1017/s0305004100017163.

[71] Y. Tsuji, K. Yoshizawa, Effects of electron-phonon coupling on quantum interference in polyenes, J. Chem. Phys. 149 (13) (2018) 134115, http://dx.doi.org/10.1063/1.5048955.

[72] Y. Tsuji, E. Estrada, R. Movassagh, R. Hoffmann, Quantum interference, graphs, walks, and polynomials, Chem. Rev. 118 (10) (2018) 4887–4911, http://dx.doi.org/10.1021/acs.chemrev.7b00733.

[73] M. Niţă, M. Ţolea, D.C. Marinescu, Conductance zeros in complex molecules and lattices from the interference set method, Phys. Rev. B 103 (2021) 125307, http://dx.doi.org/10.1103/PhysRevB.103.125307, URL https://link.aps.org/doi/10.1103/PhysRevB.103.125307.

[74] K.G.L. Pedersen, M. Strange, M. Leijnse, P. Hedegård, G.C. Solomon, J. Paaske, Quantum interference in off-resonant transport through single molecules, Phys. Rev. B 90 (2014) 125413, http://dx.doi.org/10.1103/PhysRevB.90.125413, URL https://link.aps.org/doi/10.1103/PhysRevB.90.125413.

[75] A. Narita, X. Feng, Y. Hernandez, S.A. Jensen, M. Bonn, H. Yang, I.A. Verzhbitskiy, C. Casiraghi, M.R. Hansen, A.H.R. Koch, G. Fytas, O. Ivasenko, B. Li, K.S. Mali, T. Balandina, S. Mahesh, S.D. Feyter, K. Müllen, Synthesis of structurally well-defined and liquid-phase-processable graphene nanoribbons, Nature Chem. 6 (2) (2013) 126–132, http://dx.doi.org/10.1038/nchem.1819.

[76] G. Gandus, A. Valli, D. Passerone, R. Stadler, Smart local orbitals for efficient calculations within density functional theory and beyond, J. Chem. Phys. 153 (19) (2020) 194103, http://dx.doi.org/10.1063/5.0021821.

[77] R. Landauer, Spatial variation of currents and fields due to localized scatterers in metallic conduction, IBM J. Res. Dev. 1 (3) (1957) 223–231, http://dx.doi.org/10.1147/rd.13.0223.

[78] C.J.O. Verzijl, J.S. Seldenthuis, J.M. Thijssen, Applicability of the wide-band limit in DFT-based molecular transport calculations, J. Chem. Phys. 138 (9) (2013) 094102, http://dx.doi.org/10.1063/1.4793259.

[79] O. Sengul, A. Valli, R. Stadler, Electrode effects on the observability of destructive quantum interference in single-molecule junctions, Nanoscale 13 (40) (2021) 17011–17021, http://dx.doi.org/10.1039/d1nr01230d.

[80] M.G. Reuter, T. Hansen, Communication: Finding destructive interference features in molecular transport junctions, J. Chem. Phys. 141 (18) (2014) 181103, http://dx.doi.org/10.1063/1.4901722.

[81] Y. Tsuji, R. Hoffmann, R. Movassagh, S. Datta, Quantum interference in polyenes, J. Chem. Phys. 141 (22) (2014) 224311, http://dx.doi.org/10.1063/1.4903043.

[82] P. Sam-ang, M.G. Reuter, Characterizing destructive quantum interference in electron transport, New J. Phys. 19 (5) (2017) 053002, http://dx.doi.org/10.1088/1367-2630/aa6c23.

[83] Y.-W. Son, M.L. Cohen, S.G. Louie, Energy gaps in graphene nanoribbons, Phys. Rev. Lett. 97 (2006) 216803, http://dx.doi.org/10.1103/PhysRevLett.97.216803, URL https://link.aps.org/doi/10.1103/PhysRevLett.97.216803.

[84] A.D. Güçlü, P. Potasz, P. Hawrylak, Excitonic absorption in gate-controlled graphene quantum dots, Phys. Rev. B 82 (2010) 155445, http://dx.doi.org/10.1103/PhysRevB.82.155445, URL https://link.aps.org/doi/10.1103/PhysRevB.82.155445.

[85] S.K. Singh, M. Neek-Amal, F.M. Peeters, Electronic properties of graphene nano-flakes: Energy gap, permanent dipole, termination effect, and Raman spectroscopy, J. Chem. Phys. 140 (7) (2014) 074304, http://dx.doi.org/10.1063/1.4865414.

[86] R. Miao, H. Xu, M. Skripnik, L. Cui, K. Wang, K.G.L. Pedersen, M. Leijnse, F. Pauly, K. Wärnmark, E. Meyhofer, P. Reddy, H. Linke, Influence of quantum interference on the thermoelectric properties of molecular junctions, Nano Lett. 18 (9) (2018) 5666–5672, http://dx.doi.org/10.1021/acs.nanolett.8b02207.

[87] M.H. Garner, G.C. Solomon, Simultaneous suppression of π- and σ-transmission in π-conjugated molecules, J. Phys. Chem. Lett. 11 (17) (2020) 7400–7406, http://dx.doi.org/10.1021/acs.jpclett.0c01727.

[88] P.Y. Huang, C.S. Ruiz-Vargas, A.M. van der Zande, W.S. Whitney, M.P. Levendorf, J.W. Kevek, S. Garg, J.S. Alden, C.J. Hustedt, Y. Zhu, J. Park, P.L. McEuen, D.A. Muller, Grains and grain boundaries in single-layer graphene atomic patchwork quilts, Nature 469 (7330) (2011) 389–392, http://dx.doi.org/10.1038/nature09718.

[89] N.J.G. Couto, D. Costanzo, S. Engels, D.-K. Ki, K. Watanabe, T. Taniguchi, C. Stampfer, F. Guinea, A.F. Morpurgo, Random strain fluctuations as dominant disorder source for high-quality on-substrate graphene devices, Phys. Rev. X 4 (2014) 041019, http://dx.doi.org/10.1103/PhysRevX.4.041019, URL https://link.aps.org/doi/10.1103/PhysRevX.4.041019.

[90] L. Banszerus, M. Schmitz, S. Engels, M. Goldsche, K. Watanabe, T. Taniguchi, B. Beschoten, C. Stampfer, Ballistic transport exceeding 28 μm in CVD grown graphene, Nano Lett. 16 (2) (2016) 1387–1391, http://dx.doi.org/10.1021/acs.nanolett.5b04840.

[91] S. Datta, Quantum Transport, Cambridge University Press, Cambridge, England, 2005.

[92] K.S. Thygesen, A. Rubio, Conserving GW scheme for nonequilibrium quantum transport in molecular contacts, Phys. Rev. B 77 (2008) 115333, http://dx.doi.org/10.1103/PhysRevB.77.115333, URL https://link.aps.org/doi/10.1103/PhysRevB.77.115333.

[93] M. Strange, C. Rostgaard, H. Häkkinen, K.S. Thygesen, Self-consistent GW calculations of electronic transport in thiol- and amine-linked molecular junctions, Phys. Rev. B 83 (2011) 115108, http://dx.doi.org/10.1103/PhysRevB.83.115108, URL https://link.aps.org/doi/10.1103/PhysRevB.83.115108.

[94] T. Markussen, K.S. Thygesen, Temperature effects on quantum interference in molecular junctions, Phys. Rev. B 89 (2014) 085420, http://dx.doi.org/10.1103/PhysRevB.89.085420, URL https://link.aps.org/doi/10.1103/PhysRevB.89.085420.

[95] D. Jacob, Towards a full ab initio theory of strong electronic correlations in nanoscale devices, J. Phys.: Condens. Matter 27 (24) (2015) 245606, http://dx.doi.org/10.1088/0953-8984/27/24/245606.

[96] C.M. Kropf, A. Valli, P. Franceschini, G.L. Celardo, M. Capone, C. Giannetti, F. Borgonovi, Towards high-temperature coherence-enhanced transport in heterostructures of a few atomic layers, Phys. Rev. B 100 (2019) 035126, http://dx.doi.org/10.1103/PhysRevB.100.035126, URL https://link.aps.org/doi/10.1103/PhysRevB.100.035126.

[97] A. Droghetti, M.M. Radonjić, A. Halder, I. Rungger, L. Chioncel, DFT + Σ_2 Method for electron correlation effects at transition metal surfaces, Phys. Rev. B 105 (2022) 115129, http://dx.doi.org/10.1103/PhysRevB.105.115129, URL https://link.aps.org/doi/10.1103/PhysRevB.105.115129.

[98] A. Droghetti, M.M. Radonjić, L. Chioncel, I. Rungger, Dynamical mean-field theory for spin-dependent electron transport in spin-valve devices, Phys. Rev. B 106 (7) (2022) http://dx.doi.org/10.1103/physrevb.106.075156.

[99] R.G. Parr, D.P. Craig, I.G. Ross, Molecular orbital calculations of the lower excited electronic levels of benzene, configuration interaction included, J. Chem. Phys. 18 (12) (1950) 1561–1563, http://dx.doi.org/10.1063/1.1747540.

[100] R. Pariser, R.G. Parr, A semi-empirical theory of the electronic spectra and electronic structure of complex unsaturated molecules. I, J. Chem. Phys. 21 (3) (1953) 466–471, http://dx.doi.org/10.1063/1.1698929.

[101] J.A. Pople, Electron interaction in unsaturated hydrocarbons, Trans. Faraday Soc. 49 (1953) 1375, http://dx.doi.org/10.1039/tf9534901375.

[102] M. Schüler, M. Rösner, T.O. Wehling, A.I. Lichtenstein, M.I. Katsnelson, Optimal hubbard models for materials with nonlocal Coulomb interactions: Graphene, silicene, and benzene, Phys. Rev. Lett. 111 (2013) 036601, http://dx.doi.org/10.1103/PhysRevLett.111.036601, URL https://link.aps.org/doi/10.1103/PhysRevLett.111.036601.

[103] P. Pudleiner, P. Thunström, A. Valli, A. Kauch, G. Li, K. Held, Parquet approximation for molecules: Spectrum and optical conductivity of the Pariser-parr-pople model, Phys. Rev. B 99 (2019) 125111, http://dx.doi.org/10.1103/PhysRevB.99.125111, URL https://link.aps.org/doi/10.1103/PhysRevB.99.125111.

[104] C. Weber, A. Amaricci, M. Capone, P.B. Littlewood, Augmented hybrid exact-diagonalization solver for dynamical mean field theory, Phys. Rev. B 86 (2012) 115136, http://dx.doi.org/10.1103/PhysRevB.86.115136, URL https://link.aps.org/doi/10.1103/PhysRevB.86.115136.

[105] A. Amaricci, L. Crippa, A. Scazzola, F. Petocchi, G. Mazza, L. de Medici, M. Capone, EDIpack: A parallel exact diagonalization package for quantum impurity problems, Comput. Phys. Comm. 273 (2022) 108261, http://dx.doi.org/10.1016/j.cpc.2021.108261.

[106] A. Valli, A. Amaricci, A. Toschi, T. Saha-Dasgupta, K. Held, M. Capone, Effective magnetic correlations in hole-doped graphene nanoflakes, Phys. Rev. B 94 (2016) 245146, http://dx.doi.org/10.1103/PhysRevB.94.245146, URL https://link.aps.org/doi/10.1103/PhysRevB.94.245146.

[107] K. Baumann, A. Valli, A. Amaricci, M. Capone, Inducing and controlling magnetism in the honeycomb lattice through a harmonic trapping potential, Phys. Rev. A 101 (2020) 033611, http://dx.doi.org/10.1103/PhysRevA.101.033611, URL https://link.aps.org/doi/10.1103/PhysRevA.101.033611.

[108] A. Valli, T. Schäfer, P. Thunström, G. Rohringer, S. Andergassen, G. Sangiovanni, K. Held, A. Toschi, Dynamical vertex approximation in its parquet implementation: Application to Hubbard nanorings, Phys. Rev. B 91 (2015) 115115, http://dx.doi.org/10.1103/PhysRevB.91.115115, URL https://link.aps.org/doi/10.1103/PhysRevB.91.115115.

[109] M. Sentef, J. Kuneš, P. Werner, A.P. Kampf, Correlations in a band insulator, Phys. Rev. B 80 (2009) 155116, http://dx.doi.org/10.1103/PhysRevB.80.155116, URL https://link.aps.org/doi/10.1103/PhysRevB.80.155116.

[110] M. Snoek, I. Titvinidze, C. Tőke, K. Byczuk, W. Hofstetter, Antiferromagnetic order of strongly interacting fermions in a trap: real-space dynamical mean-field analysis, New J. Phys. 10 (9) (2008) 093008, http://dx.doi.org/10.1088/1367-2630/10/9/093008.

[111] D. Jacob, K. Haule, G. Kotliar, Dynamical mean-field theory for molecular electronics: Electronic structure and transport properties, Phys. Rev. B 82 (2010) 195115, http://dx.doi.org/10.1103/PhysRevB.82.195115, URL https://link.aps.org/doi/10.1103/PhysRevB.82.195115.

[112] A. Valli, G. Sangiovanni, O. Gunnarsson, A. Toschi, K. Held, Dynamical vertex approximation for nanoscopic systems, Phys. Rev. Lett. 104 (2010) 246402, http://dx.doi.org/10.1103/PhysRevLett.104.246402, URL https://link.aps.org/doi/10.1103/PhysRevLett.104.246402.

[113] H. Das, G. Sangiovanni, A. Valli, K. Held, T. Saha-Dasgupta, Size control of charge-orbital order in half-doped manganite $La_{0.5}Ca_{0.5}MnO_3$, Phys. Rev. Lett. 107 (2011) 197202, http://dx.doi.org/10.1103/PhysRevLett.107.197202, URL https://link.aps.org/doi/10.1103/PhysRevLett.107.197202.

[114] A. Valli, G. Sangiovanni, A. Toschi, K. Held, Correlation effects in transport properties of interacting nanostructures, Phys. Rev. B 86 (2012) 115418, http://dx.doi.org/10.1103/PhysRevB.86.115418, URL https://link.aps.org/doi/10.1103/PhysRevB.86.115418.

[115] A. Valli, H. Das, G. Sangiovanni, T. Saha-Dasgupta, K. Held, Tunable site- and orbital-selective mott transition and quantum confinement effects in $La_{0.5}Ca_{0.5}MnO_3$ nanoclusters, Phys. Rev. B 92 (2015) 115143, http://dx.doi.org/10.1103/PhysRevB.92.115143, URL https://link.aps.org/doi/10.1103/PhysRevB.92.115143.

[116] M. Schüler, S. Barthel, T. Wehling, M. Karolak, A. Valli, G. Sangiovanni, Realistic theory of electronic correlations in nanoscopic systems, Eur. Phys. J. Spec. Top. 226 (11) (2017) 2615–2640, http://dx.doi.org/10.1140/epjst/e2017-70049-3.

[117] A. Amaricci, L. Privitera, F. Petocchi, M. Capone, G. Sangiovanni, B. Trauzettel, Edge state reconstruction from strong correlations in quantum spin hall insulators, Phys. Rev. B 95 (2017) 205120, http://dx.doi.org/10.1103/PhysRevB.95.205120, URL https://link.aps.org/doi/10.1103/PhysRevB.95.205120.

[118] A. Amaricci, A. Valli, G. Sangiovanni, B. Trauzettel, M. Capone, Coexistence of metallic edge states and antiferromagnetic ordering in correlated topological insulators, Phys. Rev. B 98 (2018) 045133, http://dx.doi.org/10.1103/PhysRevB.98.045133, URL https://link.aps.org/doi/10.1103/PhysRevB.98.045133.

[119] L. Chioncel, C. Morari, A. Östlin, W.H. Appelt, A. Droghetti, M.M. Radonjić, I. Rungger, L. Vitos, U. Eckern, A.V. Postnikov, Transmission through correlated Cu_nCoCu_n heterostructures, Phys. Rev. B 92 (2015) 054431, http://dx.doi.org/10.1103/PhysRevB.92.054431, URL https://link.aps.org/doi/10.1103/PhysRevB.92.054431.

[120] T.T. Phùng, R. Peters, A. Honecker, G. Trambly de Laissardière, J. Vahedi, Spin-caloritronic transport in hexagonal graphene nanoflakes, Phys. Rev. B 102 (2020) 035160, http://dx.doi.org/10.1103/PhysRevB.102.035160, URL https://link.aps.org/doi/10.1103/PhysRevB.102.035160.

[121] A. Ferretti, A. Calzolari, R.D. Felice, F. Manghi, First-principles theoretical description of electronic transport including electron-electron correlation, Phys. Rev. B 72 (12) (2005) http://dx.doi.org/10.1103/physrevb.72.125114.

[122] Y. Meir, N.S. Wingreen, Landauer formula for the current through an interacting electron region, Phys. Rev. Lett. 68 (1992) 2512–2515, http://dx.doi.org/10.1103/PhysRevLett.68.2512, URL https://link.aps.org/doi/10.1103/PhysRevLett.68.2512.

[123] H. Ness, L.K. Dash, R.W. Godby, Generalization and applicability of the Landauer formula for nonequilibrium current in the presence of interactions, Phys. Rev. B 82 (2010) 085426, http://dx.doi.org/10.1103/PhysRevB.82.085426, URL https://link.aps.org/doi/10.1103/PhysRevB.82.085426.

[124] A. Droghetti, I. Rungger, Quantum transport simulation scheme including strong correlations and its application to organic radicals adsorbed on gold, Phys. Rev. B 95 (2017) 085131, http://dx.doi.org/10.1103/PhysRevB.95.085131, URL https://link.aps.org/doi/10.1103/PhysRevB.95.085131.

[125] A. Valli, J.M. Tomczak, Resistance saturation in semi-conducting polyacetylene molecular wires, J. Computational Electronics (2023) http://dx.doi.org/10.1007/s10825-023-02043-7.

[126] D.C. Elias, R.V. Gorbachev, A.S. Mayorov, S.V. Morozov, A.A. Zhukov, P. Blake, L.A. Ponomarenko, I.V. Grigorieva, K.S. Novoselov, F. Guinea, A.K. Geim, Dirac cones reshaped by interaction effects in suspended graphene, Nat. Phys. 7 (9) (2011) 701–704, http://dx.doi.org/10.1038/nphys2049.

[127] A. Amaricci, L. de' Medici, G. Sordi, M.J. Rozenberg, M. Capone, Path to poor coherence in the periodic Anderson model from Mott physics and hybridization, Phys. Rev. B 85 (2012) 235110, http://dx.doi.org/10.1103/PhysRevB.85.235110, URL https://link.aps.org/doi/10.1103/PhysRevB.85.235110.

[128] M. Wais, J. Kaufmann, M. Battiato, K. Held, Comparing scattering rates from Boltzmann and dynamical mean-field theory, Phys. Rev. B 103 (2021) 205141, http://dx.doi.org/10.1103/PhysRevB.103.205141, URL https://link.aps.org/doi/10.1103/PhysRevB.103.205141.

[129] G. Gandus, D. Passerone, R. Stadler, M. Luisier, A. Valli, Strongly correlated physics in organic open-shell quantum systems, 2023, http://dx.doi.org/10.48550/ARXIV.2301.00282, arXiv, URL https://arxiv.org/abs/2301.00282.

[130] O.V. Yazyev, R.B. Capaz, S.G. Louie, Theory of magnetic edge states in chiral graphene nanoribbons, Phys. Rev. B 84 (2011) 115406, http://dx.doi.org/10.1103/PhysRevB.84.115406, URL https://link.aps.org/doi/10.1103/PhysRevB.84.115406.

[131] T. Gunst, T. Markussen, K. Stokbro, M. Brandbyge, Inelastic vibrational signals in electron transport across graphene nanoconstrictions, Phys. Rev. B 93 (2016) 245415, http://dx.doi.org/10.1103/PhysRevB.93.245415, URL https://link.aps.org/doi/10.1103/PhysRevB.93.245415.

[132] V. Rabache, J. Chaste, P. Petit, M.L.D. Rocca, P. Martin, J.-C. Lacroix, R.L. McCreery, P. Lafarge, Direct observation of large quantum interference effect in anthraquinone solid-state junctions, J. Am. Chem. Soc. 135 (28) (2013) 10218–10221, http://dx.doi.org/10.1021/ja403577u.

[133] A.A. Bakulin, R. Lovrincic, X. Yu, O. Selig, H.J. Bakker, Y.L.A. Rezus, P.K. Nayak, A. Fonari, V. Coropceanu, J.-L. Brédas, D. Cahen, Mode-selective vibrational modulation of charge transport in organic electronic devices, Nature Commun. 6 (2015) 7880, http://dx.doi.org/10.1038/ncomms8880.

[134] J. van der Lit, M.P. Boneschanscher, D. Vanmaekelbergh, M. Ij"as, A. Uppstu, M. Ervasti, A. Harju, P. Liljeroth, I. Swart, Suppression of electron-vibron coupling in graphene nanoribbons contacted via a single atom, Nature Commun. 4 (2013) 2023, http://dx.doi.org/10.1038/ncomms3023.

[135] S.Y. Davydov, Estimation of the electron–phonon coupling constants for graphene and metallic and nonmetallic substrates, Phys. Solid State 60 (4) (2018) 812–820, http://dx.doi.org/10.1134/s1063783418040054.